Island Arc (2009) **18**, 404–427

Thematic Article

Sediment sequences and paleosols in the Kyichu Valley, southern Tibet (China), indicating Late Quaternary environmental changes

KNUT KAISER,[1]* ZHONGPING LAI,[2] BIRGIT SCHNEIDER,[3] WERNER H. SCHOCH,[4] XUHUI SHEN,[5] GEORG MIEHE[1] AND HELMUT BRÜCKNER[1]

[1]*Faculty of Geography, University of Marburg, 35032 Marburg, Germany,* [2]*Qinghai Institute of Salt Lakes, Chinese Academy of Sciences, 810008 Xining, China,* [3]*Department of Geography, University of Leipzig, 04103 Leipzig, Germany,* [4]*Laboratory of Quaternary Woods, 8135 Langnau, Switzerland, and* [5]*Laboratory for Earthquake Observation from Space, China Earthquake Administration, 100036 Beijing, China*

Abstract The Tibetan Plateau is highly sensitive to environmental changes and affects the settings of a far larger territory in Central Asia and beyond. Thus, knowledge on past environmental changes in that area is essential. Even though the Kyichu (Lhasa River) Valley and its tributaries is an easily accessible area, the Late Quaternary landscape evolution of southern Tibet is in general scarcely known. Therefore, 12 sedimentary sections in the middle and lower catchment were subjected to multidisciplinary analyses (sedimentology, paleopedology, AMS ^{14}C and luminescence dating, and charcoal determination) aiming at results on regional paleoenvironmental changes. At the altitude studied (3600–4000 m above sealevel), no glacial relics could be detected, indicating that the valley positions have been unglaciated since the Last Interglacial. The lack of fluvial–lacustrine structures above the floodplain is due to the aggradational character of this tectonically (sub-)active valley, which caused an alluvial burying of older valley bottoms. During the Late Pleistocene the mouth area of the Kyichu was occupied by a lake which was part of a larger dam-lake in the superordinate Yarlung Zhangbo Valley. On the valley flanks, loesses were predominantly deposited before the Last Glacial Maximum (LGM), whereas eolian sands were predominantly deposited around and after the LGM. Paleosols of Last Interglacial, Last Glacial and Holocene ages regularly occur at terrestrial sites representing temperate to cool and humid to semiarid conditions during soil formation. Ages of colluvial sediments indicate that the widespread barren valley slopes were primarily formed by Late Pleistocene erosion followed by a secondary Holocene erosion phase. Charcoal spectra indicate a Late Holocene change from a forest environment to a pastoral environment with sparse grasses, herbs and dwarf shrubs. It is assumed that the Late Holocene environmental changes, such as loss of forests/woodlands and erosion, have at least been reinforced by humans, enhancing a regional climatic aridification and cooling trend.

Key words: colluvial, eolian, fluvial, lacustrine, Lhasa River.

INTRODUCTION

In the last two decades, much scientific effort has been devoted to studying the Late Quaternary climate history and paleoenvironmental change of the Tibetan Plateau, as this largest alpine area in the world (~2.2×10^6 km^2) affects the settings of a far larger territory in Central Asia and beyond. Thus, future climate-driven and human-induced changes on the plateau (e.g. Du *et al*. 2004; Böhner & Lehmkuhl 2005; Cui *et al*. 2006) will inevitably cause environmental consequences in the surroundings. For example, landcover changes can alter the discharge and suspended load of major

*Correspondence: Faculty of Geography, University of Marburg, Deutschhaustrasse 10, 35032 Marburg, Germany (email: knut.kaiser@gmx.net)

Received 28 August 2007; accepted for publication 15 January 2008.

doi:10.1111/j.1440-1738.2008.00629.x

rivers having their sources on the Plateau, such as Huang He, Yangtze, Brahmaputra, Mekong, and Salween. A possible aridification can increase the dust production, which will be partly deposited as loess on the adjacent Chinese Loess Plateau and beyond. Furthermore, but hardly predictable so far, changes in the energy balance on the Tibetan Plateau will have a significant impact on the regional to continental climate, and might have an impact on the global climate (Cui *et al.* 2006; Fan *et al.* 2007). Therefore, the regional feedbacks and interactions between relief, soil, and climatic and biotic systems of different areal and temporal scales must be understood. This necessarily requires the consideration of paleoenvironmental conditions, which provide exemplary insights into the past interplay of these systems.

In general, as sediments and soils were formed under the influence of geologic, geomorphologic, climatic, biotic and, at least for certain periods, human factors, they can be used to indicate past environments. So far, Quaternary research on the Tibetan Plateau has mainly focused on changes in the East Asian monsoon system, on vegetation changes, and on glacial history (e.g. Thompson *et al.* 2000; Lehmkuhl & Owen 2005; Herzschuh 2006). However, several geologic–geomorphic processes, such as eolian and paleohydrological events, as well as the Holocene impact of man are only rudimentarily known (e.g. Lehmkuhl & Haselein 2000; Aldenderfer & Zhang 2004; Morrill *et al.* 2006; Kaiser *et al.* 2007).

Most paleoenvironmental records on the Tibetan Plateau have been based on lacustrine sediments, which often yielded long-term and continuous data sets (e.g. Overpeck *et al.* 2005; Herzschuh *et al.* 2006; Wu *et al.* 2006). In contrast, comparatively few records from terrestrial sites, such as loess–paleosol sequences, eolian sands or moraines, have been considered (e.g. Küster *et al.* 2006; Li *et al.* 2006; Owen *et al.* 2006) because terrestrial sites, except modern glaciers (e.g. Thompson *et al.* 2000), mostly represent discontinuous sequences yielding only fragmentary paleoenvironmental information. However, certain kinds of information are obtainable almost only from terrestrial archives, such as on slope erosion, eolian dynamics, and glacial processes. Furthermore, since most of the modern lakes on the Tibetan Plateau did not start their sedimentation until the Late Glacial (Herzschuh 2006), terrestrial sequences comprising fossil lacustrine and non-lacustrine sediments are essential sources for information before *ca* 15 000 cal BP.

Even though the Lhasa area is easily accessible, the Late Quaternary landscape evolution of southern Tibet is in general astonishingly scarcely known. For instance, data on the genesis of the fluvial and eolian relief as well as on paleoenvironmental changes are rare (e.g. Tang *et al.* 2000; Zhang 2001; Montgomery *et al.* 2004; Sun *et al.* 2007). Therefore, a research project on the Holocene geomorphic genesis of the Kyichu (Lhasa River) catchment was launched to clarify the more recent geomorphic and paleoenvironmental history, continuing previous research on past human–environment relationships in that area (Kaiser *et al.* 2006; Miehe *et al.* 2006). According to sedimentary sequences recorded in 2006 and their subsequent geochronological analysis, the temporal focus has now be expanded to the Last Interglacial comprising the last *ca* 100 000 years. For the first time in southern Tibet, Interglacial and Last Glacial paleosol-bearing terrestrial sequences were detected and analyzed on a larger scale.

The overall question to be addressed by this study is what sediments and paleosols can indicate about Late Quaternary environmental changes in southern Tibet. To this end, the following aspects will be pursued: (i) exemplary presentation of paleosol-bearing fluvial–lacustrine, eolian, and colluvial sequences and their characterization by means of sedimentological, pedological, geochronological, and botanical analyses; and (ii) interpretation and discussion of the results with respect to regional environmental changes.

STUDY AREA

The Kyichu area is a sub-catchment of the east-flowing Yarlung Zhangbo (alternatively Y. Zangpo or Y. Tsangpo), which, after leaving the southeastern Himalayas, flows west to India as the Brahmaputra (Kyichu catchment = 32 588 km^2, river length = 530 km, altitude difference = 1810 m; Chinese Academic Expedition Group (1983). The undulating flow directions of the Kyichu and its tributaries follow mainly northwest–southeast, west–east, and northeast–southwest-trending tectonic structures (Figs 1,2a,b). In general, a high gradient in altitude and the geologic-tectonic setting have produced a wide variety of geomorphic processes, sediments, local climate, soils, and vegetation.

Tectonically, the Kyichu catchment belongs to the structural block of the Lhasa terrane, which

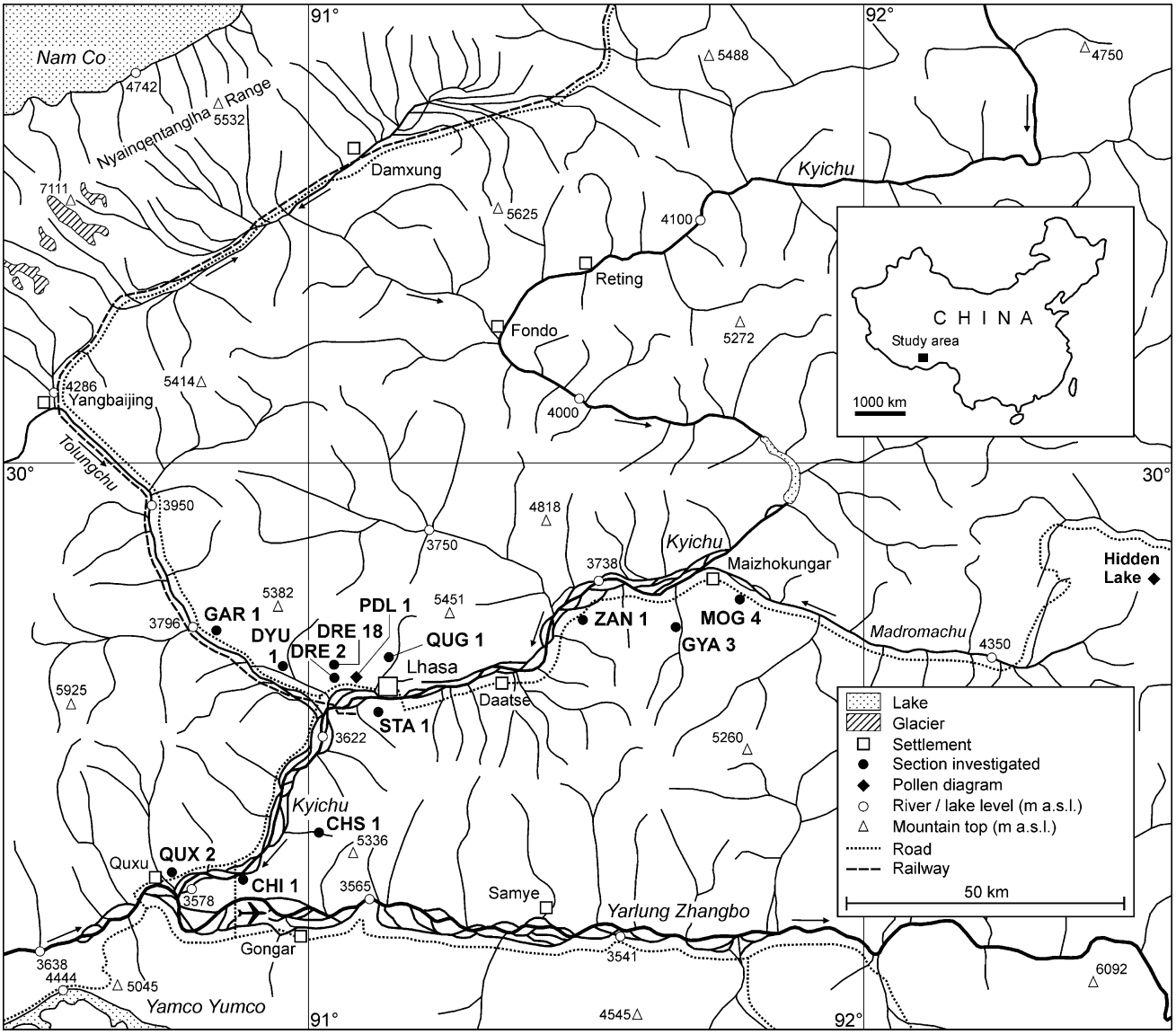

Fig. 1 River network of the Kyichu and adjacent catchment areas with the sections recorded (map adapted from Institute of Geography, Chinese Academy of Sciences 1990). a.s.l., above sealevel.

was formed following the collision of the Indian and Eurasian plates in the early Tertiary (Eocene/Oligocene boundary *ca* 55 Ma according to most workers, e.g. Klootwijk *et al*. 1992; Rowley 1996; or *ca* 34 Ma according to Aitchison *et al*. 2007). The upper and middle valley sections of the Kyichu as well as its tributaries follow strike-slip faults, whereas the mouth area belongs to the Tsangpo suture (Zhang 1998). The predominant rock in the study area is granite accompanied by Carboniferous to Tertiary metamorphics and sediments, which are covered outside the valleys and basins by a thin veneer of Quaternary eolian and colluvial sediments (Institute of Geography, Chinese Academy of Sciences 1990; Fig. 2b). Larger areas of active eolian sands exist on the valley flanks in the river mouth area adjoining the Yarlung Zhangbo Valley (Fig. 3c). According to Lehmkuhl *et al*. (2002), southern Tibet is characterized vertically by the following geomorphic zones: (i) zone of fluvial processes and sand fields/dunes (up to ~3800 m above sealevel [a.s.l.]); (ii) zone of torrent valleys and gully erosion (up to ~4200 m a.s.l.); (iii) zone of steppe gullies (up to ~5100 m a.s.l.); and (iv) zone of periglacial processes (above ~5100 m a.s.l.). The recent snowline is calculated at about 6000 m a.s.l. However, during the Pleistocene glacial stages the snowline was lowered by about 300–800 m (Lehmkuhl *et al*. 2002). For the lower Kyichu area, traces of Pleistocene

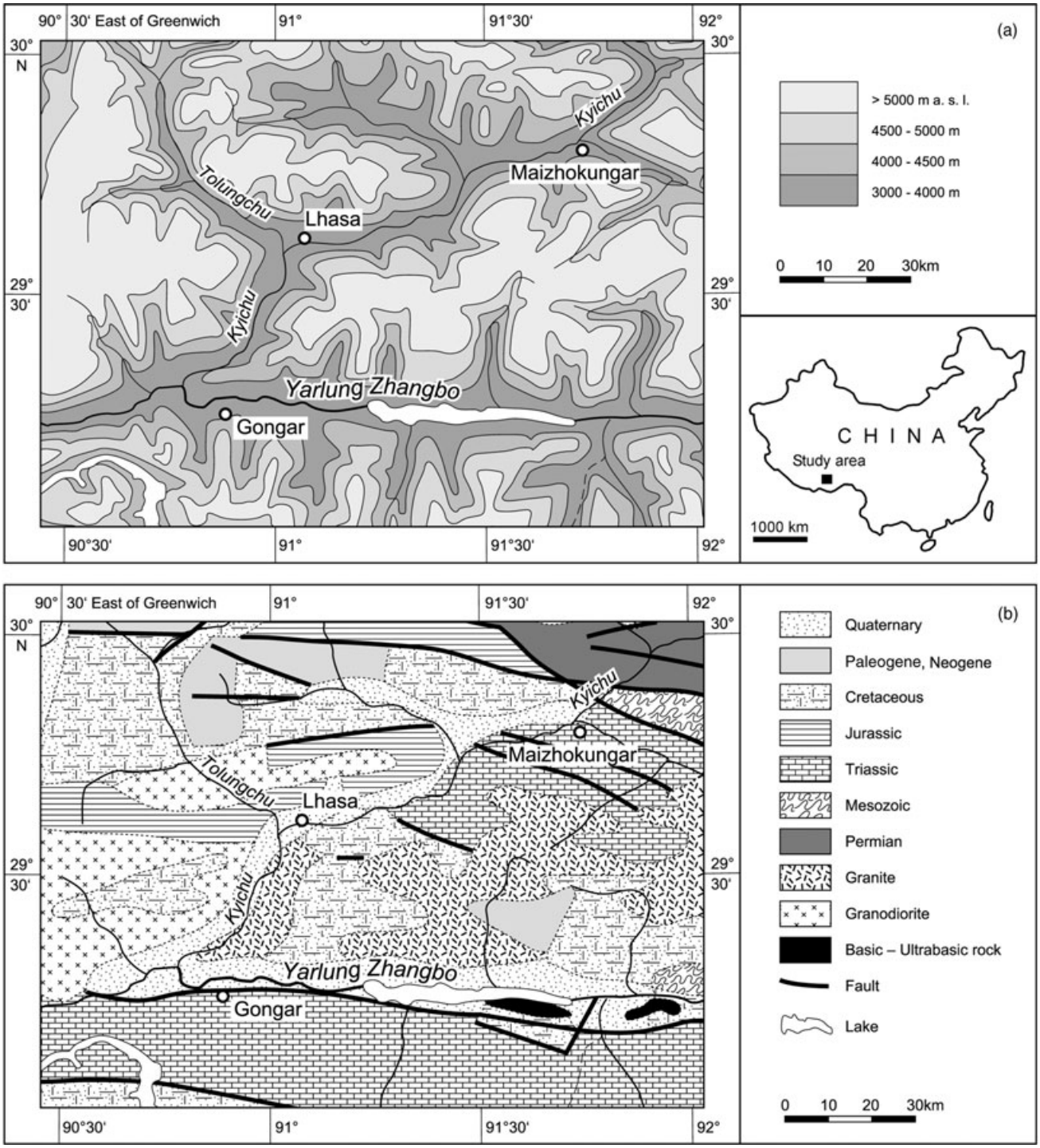

Fig. 2 Study area, (a) topographic map (adapted from Miehe *et al.* 2001), (b) geological map (adapted from Institute of Geography, Chinese Academy of Sciences 1990). a.s.l., above sealevel.

glaciations are reported from the northern surroundings of Lhasa, comprising morainic deposits associated with outwash cones (~4250 and 3950 m a.s.l., precise age unknown; Kuhle (2005).

There are many headwater streams and rivers in the up to the 7117-m a.s.l.-high Nyainqentanglha Range and in the gently rolling hills around Damxung and Nagqu (~4000–5000 m a.s.l.; Fig. 1). The middle reach between Reting and Maizhokungar comprises a floodplain level of 4100–3800 m a.s.l. predominantly showing (large-scale) meandering with local anastomozing

Fig. 3 Photographs of selected sites investigated. (a) Reting site in the middle Kyichu Valley representing a relic juniper forest on a south-facing mountain slope (~4200 to 4750 m a.s.l., west of the Reting Monastery), (b) braiding floodplain of the Kyichu in the middle river course next to Maizhokungar, (c) Lower Kyichu Valley about 50 km southwest of Lhasa (next to CHI 1 section; view from ~3800 m a.s.l. towards the northeast), (d) Lhasa Basin with a large swamp in the foreground (~3650 m a.s.l., view towards southeast). The snow-covered mountain ridge in the background reaches about 5300 m a.s.l, (e) alluvial fan dissected by gullies in a side valley of the Kyichu next to Lhasa–Drepung (section DRE 18, ~3700 m a.s.l., view towards northwest), (f) barren rock and slope sediments at site GAR 1 (valley flank of the Tolungchu, ~3800 m a.s.l., view towards northeast).

and braiding sections (Fig. 3b). In this area the maximum width of the valley is 1–3 km. Northeast of Maizhokungar, a larger valley section has been flooded by an anthropogenic dam-lake in recent years. The middle and lower river course from Maizhokungar to the mouth, in particular downvalley from Lhasa, predominantly shows braiding with local anastomozing sections (Fig. 3c). The middle and lower valley sections have widths of 2–4 km comprising some larger basins, such as the Lhasa Basin (~3650 m a.s.l.), whose north–south dimension reaches about 6 km (Fig. 3d). In the Lhasa area, the mean annual discharge of the Kyichu amounts to 283 m^3/s having a strong seasonal peak in the summer (Chinese Academic Expedition Group 1983). Along the course of the Kyichu, river terraces of both aggradation (accumulation) type and degradation (erosion) type are developed only in the headwaters and the middle course up to ~ 30 km downstream of Fondo. Their surfaces reach up to about 20–30 m above the present floodplain. There exists one valley terrace in the river mouth area next to Quxu (section QUX 2) representing a very small remnant of mainly fluvial–lacustrine sediments lying about 20 m above the present Kyichu floodplain. In the middle river course between Maizhokungar and Daatse, several alluvial fans coming from the side valleys were truncated in the past by the Kyichu and present a terrace-like appearance. In contrast, in the lower river course between Lhasa and Quxu, most alluvial fans smoothly descend to the floodplain, i.e. without any visible erosional step.

So far, information on the valley fill is available from the Lhasa Basin only. According to geophysical transects and one borehole including several sedimentological and biostratigraphical analyses, three units of Quaternary sediments were differentiated filling up the approximately 6-km-wide basin (Shen *et al.* 2007; Fig. 4). The basin was

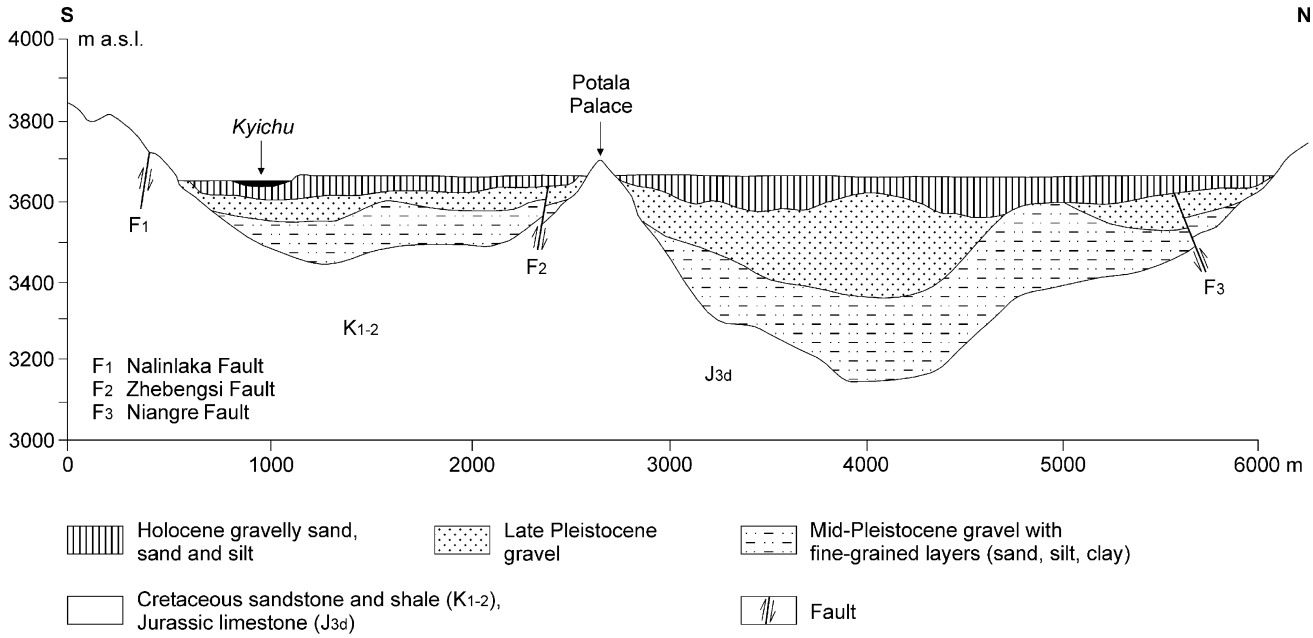

Fig. 4 Cross-section through the Lhasa Basin according to geophysical data (adapted from Shen *et al.* 2007).

initially formed in the Mid-Pleistocene containing a maximal sediment fill of about 500 m. The Kyichu Valley around Lhasa is located in the so-called Nalinlaka Fault zone, which extends over about 70 km in an east–west direction (Liu *et al.* 2007).

Pedologically, the Lhasa area belongs to the zone of 'cold calcic soils, brown calcic soils and aga soils' of southern Tibet (Institute of Geography, Chinese Academy of Sciences 1990). The local altitude-dependent soil distribution is known from a transect in the surroundings of Lhasa–Drepung (Kaiser *et al.* 2006). The permanently active floodplain of the Kyichu is characterized by mobile cobbles to sands. Temporarily active or inactive parts of the floodplain have Gleysols and Fluvisols developed from fluvial sands and silts. Chernozems and Calcaric Cambisols occur on inactive parts of alluvial fans, footslopes, and lower slopes. The middle slopes are dominated by Cambisols developed from loesses. Locally, Gleysols occur at stream sites and wet slope niches. Leptosols and barren rock associated with inactive and active periglacial forms follow on the upper slopes and top positions.

The present climate on the valley ground in Lhasa (~3650 m a.s.l.) is characterized by a mean annual air temperature (MAAT) of 7.7°C, summer temperatures of more than 15.5°C and winter temperatures below –2.1°C as well as a mean annual precipitation (MAP) of 443 mm (Domrös & Peng 1988; Miehe *et al.* 2001). However, there exists a distinct altitude-dependent climatic differentiation. Exemplary rain gauge measurements in the Lhasa area yielded an extrapolated annual rainfall at 3750 m a.s.l. of 485 mm and at 4650 m a.s.l. of 715 mm (Miehe *et al.* 2003).

As (pre-) historic and recent anthropogenic influences have strongly changed the regional environment (Kaiser *et al.* 2006; Miehe *et al.* 2006), the present-day character of the study area is only seminatural. In the middle and lower reaches of the Kyichu, livestock grazing and fuel wood extraction have widely replaced the natural vegetation and left partly eroded badlands (Fig. 3e,f). The (former) floodplains are characterized either by: (i) mobile cobbles to sands sparsely overgrown by grasses; (ii) irrigated arable land and wood plantations; or (iii) grazed wetlands with a dense cover of sedges, grasses, and herbs. Only locally are grazed remains of the natural phreatophytic woodlands consisting of buckthorn (*Hippophae* spp.), willow (*Salix* spp.) and poplar (*Populus* spp.). Alluvial fans, footslopes, and middle slopes are exposed to a strong, year-round grazing impact having a grass dominated vegetation with low thorny shrubs (e.g. *Sophora moorcroftiana*) and wormwoods (*Artemisia santolinifolia*). In some safe slope positions, shrubs several meters high occur (e.g. *Buddleja* spp., *Cotoneaster* spp.). Above about 4500 m a.s.l. dense sedge mats of *Kobresia pygmaea* accompanied by cushions occur. Dry-site forests/woodlands or even trees are very rare in

the study area. The largest remains of the former forest vegetation, proven by a comprehensive survey detecting several occurrences of small-scale juniper woodlands and trees in recent years (Miehe *et al.* 2008), is a south-exposed mature juniper forest (*Juniperus tibetica*) around Reting Monastery comprising trees of 10–15 m in height and up to *ca* 1000 years in age (Miehe *et al.* 2003, 2008; Bräuning 2007; Figs 1,3a). Remains of the natural forest vegetation on north-facing slopes consisting of birch (*Betula* spp.), willow (*Salix* spp.) and rhododendron (*Rhododendron* spp.) are preserved in the middle Kyichu Valley and the upper Madromachu Valley.

METHODS

FIELD RECORDS, SEDIMENTOLOGY AND PALEOPEDOLOGY

Field research for the sections presented here mainly took place in spring 2006, except for one alluvial fan sequence (DRE 2) and two colluvial sequences (GAR 1, QUG 1), which were already recorded in 2003 (Kaiser *et al.* 2006). Both natural and anthropogenic exposures with a thickness of 2–13 m were used after preparation of the sections. The profiles were described and sampled according to an international pedological standard (FAO 2006). Designations of soil horizons and soil types are given using the 'World Reference Base for Soil Resources' (IUSS-ISRIC-FAO 2006). The content of coarse matter (>2 mm), comprising granules to boulders (Udden–Wentworth grain-size scale), was estimated in the field. All of the following analyses were performed on the matrix matter <2 mm (Table 1).

After air drying, careful hand-crushing, humus and carbonate destruction (H_2O_2 30%, HCl 10%), and dispersion with sodium pyrophosphate, a combined pipette and sieving test was used to determine the grain-size distribution. The appearing grain-size terms 'fine, medium and coarse (-grained) sand' are defined by the mesh-sizes <0.2 mm, <0.63 mm and <2.0 mm, respectively. Organic carbon (OC) was measured by dry combustion (Elementar vario EL) at 1100°C in duplicate. Samples of three sections, however (OC analysis was not possible), were treated by burning for two hours at 550°C to determine the loss-on-ignition (LOI), yielding an estimate for the organic content. The LOI gives an overestimation for the organic matter (e.g. for silts ~2%, according to own experience), which is caused by water bound in minerals and oxides. $CaCO_3$ was determined volumetrically. Soil pH was analyzed potentiometrically in 0.01 M $CaCl_2$ (soil/solution ratio = 1:2.5). Electrical conductivity (EC) was measured by means of an electrode in distilled water (soil/solution ratio = 1:2.5).

PALEOBOTANY

Charcoal and fossil wood originating from paleosols and various sediments were analyzed to provide both matter for radiocarbon dating and for paleoecological information. Charcoal and fossil wood were extracted macroscopically from the sections comprising pieces up to 2 cm in length but normally being only 1–5 mm in size. Exact identification required an inspection of microscopic features by means of comparison with preparations from living material or from photographs of transverse, radial, and tangential sections of recent wood species (Schoch 1986; Schweingruber 1990). Microscopic examination was carried out on fracture surfaces of the air-dried charcoal pieces with surface illumination and magnifications of 5–50x (Table 2). It was possible to identify almost all indigenous woods easily, although the charcoals pieces were often in some parts a glass-like, an amorphous mass, or they exploded from gas pressure during the burning process. In some cases, it is in principle not possible to determine the species: e.g. the *Juniperus* (juniper) species present in the area can not be distinguished from each other on the basis of their wood anatomy.

GEOCHRONOLOGY

Radiocarbon dating

Twelve samples of different material (charcoal, bulk-soil matter, wood, bone) were extracted from the profiles and subsequently analyzed in the Erlangen AMS Radiocarbon Laboratory (Table 3). Bulk soil samples were pre-treated by the removal of roots and the acid–alkali–acid (AAA) method (Kretschmer *et al.* 1998), to remove carbonates and mobile humic substances, which otherwise might affect the ^{14}C results. The soil organic matter fraction dated consist of *humins*, which are considered to be a reliable material for ^{14}C dating in soils (Pessenda *et al.* 2001). Further treatment of the samples followed the standard methods of the Erlangen Laboratory (Scharf *et al.* 2007).

In general, the ^{14}C ages presented in the text are calibrated (cal BP values). The calibration of the

Table 1 Sedimentological and pedological data

Sample	Altitude [m a.s.l.]	Latitude[N]	Longtitude[E]	Sampling depth [cm]	Sediment facies	Soil horizon	Color [Munsell]	Clay, silt, sand [%]	OC [%]	LOI [%]	$CaCO_3$ [%]	pH [$CaCl_2$]	EC [mS/cm]
QUX 2c	3536	29°21′57.3″	90°45′20.2″	110–160	eolian	2C	10YR6/2	3, 3, 94	0.1	–	0.0	7.9	0.050
QUX 2d				160–330	eolian	3C	10YR7/3	9, 63, 28	0.2	–	3.2	8.0	0.100
QUX 2e				330–650	lacustrine	4C	10YR7/2	10, 34, 56	0.4	–	0.0	8.0	0.080
QUX 2a				650–900	lacustrine	5C	–	32, 58, 10	0.3	–	3.5	8.0	0.120
QUX 2b				900–1000	fluvial	6C	–	4, 9, 87	0.1	–	0.6	8.0	0.050
DYU 1a	3704	29°41′19.9″	90°56′51.9″	450–470	fluvial	2Ahb	7.5YR3/2	6, 20, 74	0.4	–	0.0	7.5	0.040
DYU 1b				590–600	fluvial	3Ahb	7.5YR3/2	3, 10, 87	0.4	–	0.0	7.5	0.050
DYU 1c				690–700	fluvial	4Ahb	7.5YR3/2	8, 25, 67	0.2	–	0.0	7.4	0.020
CHS 1a	4044	29°26′36.8″	91°01′17.7″	0–40	colluvial	AhB	10YR6/3	9, 31, 60	1.1	–	0.0	6.3	0.060
CHS 1b				40–150	colluvial	C	10YR7/3	9, 26, 65	0.3	–	1.0	8.1	0.110
CHS 1c				150–170	fluvial	2Ahbg	10YR6/2	12, 29, 59	0.6	–	0.7	8.0	0.280
CHS 1d				170–255	fluvial	2Cg	10YR6/4	9, 27, 64	0.2	–	0.0	7.9	1.200
CHS 1e				255–280	fluvial	3Ahbg	10YR2/1	27, 28, 45	4.7	–	0.0	6.4	0.220
CHS 1f				280–450	fluvial	4Cg	10YR7/2	5, 23, 72	0.1	–	0.0	6.8	0.100
CHS 1g				450–485	fluvial	5Ahbg1	10YR2/2	17, 45, 38	5.5	–	0.0	2.5	3.470
CHS 1h				485–530	fluvial	5Ahbg2	2.5Y4/1	15, 62, 23	0.9	–	0.0	2.9	2.630
ZAN 1a	3705	29°46′33.9″	91°28′59.4′	0–220	fluvial-lac.	C	–	25, 48, 27	0.6	–	0.0	7.2	0.140
ZAN 1b				220–250	fluvial-lac.	Cg	–	22, 62, 16	7.3	–	0.0	7.3	0.110
DRE 2a	3654	29°40′04.6″	91°02′57.4″	0–100	colluvial-fluv.	C	10YR5/4	7, 18, 75	–	0.9	0.0	6.8	0.300
DRE 2b				100–115	fluvial	2Ahb	10YR5/2	4, 12, 84	–	4.0	0.0	6.8	0.400
DRE 2c				115–155	fluvial	2C	10YR6/4	4, 23, 73	–	1.7	0.0	6.7	0.890
MOG 4a	3894	29°47′30.0″	91°48′45.2″	0–40	colluvial	Ah	10YR4/3	14, 48, 38	1.5	–	0.0	7.3	0.160
MOG 4b				200–270	eolian	4Ck	10YR5/6	22, 52, 26	0.3	–	10.2	8.0	0.110
MOG 4c				270–290	eolian	5Bwkb	7.5YR5/6	18, 52, 30	0.3	–	13.6	8.1	0.100
MOG 4d				290–390	eolian	5C	10YR5/4	6, 46, 48	0.1	–	2.8	8.0	0.100
MOG 4e				410–670	eolian	6C	10YR5/6	11, 59, 30	0.2	–	1.5	8.0	0.080
MOG 4f				670–720	colluvial	7Ck	10YR5/4	16, 62, 22	0.3	–	4.9	8.0	0.100
MOG 4g				720–760	eolian	8BwAhkb	7.5YR3/3	20, 52, 28	0.4	–	1.0	8.0	0.110
MOG 4h				760–900	eolian	8C	2.5YR6/3	5, 57, 38	0.1	–	0.0	8.0	0.060

Table 1 *Continued*

Sample	Altitude [m a.s.l.]	Latitude[N]	Longtitude[E]	Sampling depth [cm]	Sediment facies	Soil horizon	Color [Munsell]	Clay, silt, sand [%]	OC [%]	LOI [%]	$CaCO_3$ [%]	pH [$CaCl_2$]	EC [mS/cm]
GYA 3a	3840	29°44′54.6″	91°40′02.5″	250–380	eolian	4C	10YR5/6	15, 60, 25	0.2	–	1.3	8.0	0.090
GYA 3b				380–395	eolian	5Ahkb	10YR3/3	17, 68, 15	0.5	–	1.1	7.9	0.100
GYA 3c				395–450	eolian	5C	10YR5/4	11, 67, 22	0.2	–	1.3	8.0	0.070
CHI 1d	3618	29°21′47.9″	90°53′36.0″	0–20	eolian	Ah	10YR4/3	8, 47, 45	0.2	–	0.0	7.8	0.040
CHI 1c				50–70	eolian	C	2.5Y5/3	6, 45, 49	0.1	–	0.0	7.6	0.020
CHI 1b				950–1000	eolian	C	2.5Y5/3	5, 27, 68	0.2	–	0.0	8.1	0.060
CHI 1a				1040–1050	eolian	2C	2.5Y5/3	6, 10, 84	0.2	–	0.0	8.0	0.060
STA 1a	3658	29°37°59.4″	91°05′52.0″	0–15	eolian	Ah	10YR6/3	6, 17, 77	0.5	–	0.0	7.4	0.030
STA 1b				15–135	eolian	C	10YR7/3	0, 14, 86	0.1	–	0.0	7.4	0.050
STA 1c				135–150	eolian	2Ahb	10YR3/2	4, 20, 76	0.7	–	0.0	7.4	0.020
STA 1d				150–330	eolian	2C	10YR7/3	5, 23, 72	0.1	–	0.0	7.7	0.030
DRE 18a	3707	29°40′09.7″	91°02′41.6″	0–20	colluvial	Ah	10YR5/3	10, 40, 50	1.0	–	10.1	7.8	0.110
DRE 18b				260–350	coll.-eolian	4C	10YR7/3	5, 16, 79	0.1	–	5.0	8.1	0.060
DRE 18c				350–500	eolian	5C	10YR7/3	20, 53, 27	0.3	–	15.5	8.0	0.180
DRE 18d				570–610	eolian	7B(k)wb	10YR4/4	19, 63, 18	0.2	–	3.9	8.0	0.110
DRE 18e				610–830	eolian	7C	2.5Y6/4	11, 66, 23	0.3	–	13.1	8.0	0.100
DRE 18f				830–880	eolian	8Bkwb	7.5YR5/4	14, 55, 31	0.4	–	16.8	7.9	0.110
DRE 18g				880–1000	eolian	8C	10YR5/4	12, 43, 45	0.2	–	5.1	8.0	0.100
GAR 1a	3800	29°44′25.5″	90°49′49.3″	0–3	colluvial	AhC	10YR6/3	8, 26, 66	–	2.3	0.0	5.7	0.049
GAR 1b				3–200	colluvial	C	10YR6/3	8, 15, 77	–	1.4	0.0	5.8	0.049
GAR 1c				200–208	colluvial	2AhbC	10YR3/1	12, 21, 67	–	5.8	0.0	6.0	0.078
GAR 1d				208–235	colluvial	2Cwb	10YR4/3	10, 19, 71	–	1.6	0.0	6.1	0.065
GAR 1e				235–310	colluvial	3AhbC	10YR3/2	12, 23, 65	–	2.0	0.0	6.3	0.059
GAR 1f				310–330	colluvial	3Ah/Bwb	10YR3/2	12, 20, 68	–	2.2	0.0	6.5	0.065
GAR 1g				330–350	fluvial-lac.	4C	2.5Y6/4	18, 8, 74	–	2.7	13.7	6.6	0.116
QUG 1a	3679	29°42′03.9″	91°07′42.2″	0–135	colluvial	C	10YR4/4	8, 24, 68	–	1.5	0	7.5	0.055
QUG 1b				135–170	colluvial	2Ahb	10YR5/2	9, 32, 59	–	2.5	1.1	7.3	3.510
QUG 1c				170–200	colluvial	2CBwk	2.5Y5/4	12, 29, 59	–	1.4	3.6	7.4	0.067

a.s.l., above sealevel; EC, electrical conductivity; LOI, loss on ignition; OC, organic carbon.

Table 2 Paleobotanical data

Sample	Depth [cm]	Material	Plant determined	Particles [*n*]	Proportion [%]
DYU 1b	590–600	charcoal	*Sophora* sp.	50	100.0
CHS 1e	255–280	charcoal	deciduous wood, indet.	21	58.3
			Hippophae sp.	8	22.2
			Populus sp.	5	13.9
			Caragana sp.	1	2.8
			Rosaceae/Maloideae	1	2.8
CHS 1g	450–485	wood	*Hippophae* sp.	5	100.0
ZAN 1b	220–250	charcoal	*Hippophae* sp.	50	100.0
DRE 2b	110–115	charcoal	*Juniperus* sp.	53	54.6
			Salix sp.	37	38.1
			Rhododendron sp.	3	3.1
			Hippophae sp.	2	2.1
			Rosa sp.	2	2.1
MOG 4g	720–760	charcoal	*Caragana* sp.	20	64.5
			deciduous wood, indet.	10	32.3
			Hippophae sp.	1	3.2
GYA 3b	380–395	charcoal	Rosaceae/Maloideae	20	100.0
STA 1c	135–150	charcoal	*Juniperus* sp.	30	50.8
			Sophora sp.	25	42.4
			Buddleja sp.	4	6.8
GAR 1c	200–208	charcoal	*Hippophae* sp.	91	70.5
			Rosa sp.	30	23.3
			Juniperus sp.	7	5.4
			Gramineae	1	0.8
QUG 1b	135–170	charcoal	*Hippophae* sp.	28	50.9
			Betula sp.	20	36.4
			Rosa sp.	4	7.3
			Salix sp.	2	3.6
			Spiraea sp.	1	1.8

Site information (altitudes, coordinates) is shown in Table 1.

Table 3 Radiocarbon data

Sample	Depth [cm]	Material dated	Lab. No.	$\delta^{13}C$ [‰]	^{14}C age [years BP]	^{14}C cal age [years cal BP]
DYU 1b	590–600	*Sophora* sp. charcoal	Erl-10947	–25.1	7 375 ± 67	8 196 ± 100
CHS 1e	255–280	charcoal (mixed spectrum)	Erl-10115	–24.5	5 803 ± 48	6 603 ± 59
CHS 1g	450–485	*Hippophae* sp. wood	Erl-10116	–26.7	5 964 ± 49	6 808 ± 62
ZAN 1b	220–250	*Hippophae* sp. charcoal	Erl-10941	–23.0	6 925 ± 69	7 771 ± 70
DRE 2b	100–115	*Juniperus* sp. charcoal	Erl-6776	–21.6	203 ± 41	175 ± 111
MOG 4g	720–760	charcoal (mixed spectrum)	Erl-10120	–22.6	45 682 ± 5 438	51 024 ± 6 148
GYA 3b	380–395	Rosaceae/Maloideae charcoal	Erl-10119	–24.4	44 235 ± 3 388	48 681 ± 3 786
STA 1c	135–150	*Juniperus* sp. charcoal	Erl-10940	–20.9	2 713 ± 38	2 817 ± 34
DRE 18	60–80	human bone	Erl-10125	–17.4	2 285 ± 40	2 272 ± 68
GAR 1c	200–208	*Juniperus* sp. charcoal	Erl-6782	–20.5	3 668 ± 57	4 005 ± 79
GAR 1e	250–255	bulk-soil matter (humin fraction)	Erl-8070	–21.7	7 908 ± 99	8 781 ± 152
QUG 1b	140–145	animal bone	Erl-6783	–14.8	3 053 ± 45	3 275 ± 58

Site information (altitudes, coordinates) is shown in Table 1.

^{14}C dates was performed using CalPal-2007 software (Weninger *et al.* 2007).

Luminescence dating

Luminescence dating was carried out at the Marburg Luminescence Laboratory using a Risø TL-DA 15 reader (Bøtter-Jensen *et al.* 2000). Both infrared ($\lambda = 880 \pm 80$ nm) stimulated luminescence (IRSL) of polymineral fine grains (4–11 μm) and optically stimulated luminescence (OSL, stimulation light = blue light-emitting diodes [LEDs], $\lambda = 470 \pm 20$ nm) of quartz (38–63 μm) were used. For ISRL dating, blue emission (390–

480 nm) was detected (filters Corning 7–59, Schott GG400, Schott BG39). Equivalent doses were determined using an additive dose multiple-aliquot protocol (Table 4). After irradiation, all samples were stored at room temperature for 8 weeks, preheated (16 h at 160°C) and stored for two more days. Short time fading experiments carried out on three samples revealed no signal instabilities after 4 weeks of storage (Kaiser *et al*. 2006). For quartz OSL dating, grains sized 38–63 μm were extracted (Lai & Wintle 2006; Lai *et al*. 2007). OSL signals were measured at 130°C, and recorded for 60 s through two U-340 glass filters. The single aliquot regenerative dose (SAR) protocol (Murray & Wintle 2000) was used for equivalent dose determination (preheat at 260°C for 10 s, cut-heat at 220°C for 10 s). For equivalent dose calculation, the OSL of the first 0.48 s stimulation was used (background subtracted). When calculating the environmental dose rate for OSL of middle grain-size quartz (38–63 μm), an alpha efficiency of 0.035 ± 0.003 was adopted.

The IRSL and OSL ages are indicated by ka-values. Generally, IRSL and OSL dates correlate numerically with calibrated ^{14}C ages.

RESULTS

GENERAL REMARKS

So far, about 80 sections were recorded in the middle and lower Kyichu catchment situated at various relief positions and comprising various sediments. A selection of 12 sections will be presented here, which have been already subjected to sedimentological, pedological, geochronological, and botanical analyses (Fig. 1). In the Kyichu area, on the one hand, natural sections are available in abundance due to widespread erosion processes. On the other hand, sections are often easily accessible due to numerous artificial outcrops created by intensive building and road construction as well as by extraction of raw materials. It should be mentioned here that the expansion of settlement, industry, and infrastructure, especially in the Lhasa area, has created a tremendous number of exposures in recent years.

FLUVIAL–LACUSTRINE SEQUENCES

The sequences presented can be divided into: (i) mainly lacustrine sections (QUX 2, ZAN 1); (ii) mainly fluvial sections (CHS 1); and (iii) alluvial fan sections (DYU 1, DRE 2). The fluvial deposits widely recorded lack coarser particles than granules and originate from relatively long-distance fluvial transport. In contrast, alluvial fan deposits often bear coarse particles in the form of cobbles and boulders and originate from relatively short-distance fluvial transport.

Section QUX 2 (~3600 m a.s.l., lower Kyichu Valley; Fig. 1) is cut anthropogenically in a terrace lying ~20 m above the present floodplain. The heavily dissected terrace has a lateral extension of a few hundred meters only, thus obviously representing a remnant surviving postdepositional erosion in this valley section. The 10-m-thick exposure mainly consists of silts and silty sands partly showing distinct parallel bedding/lamination (Fig. 5). Their lacustrine facies is proven by the local existence of well-developed load structures. Both $CaCO_3$ (0–3.5%) and OC (0.1–0.4%) contents are very low (Table 1). Medium-grained fluvial sand forms the base; eolian and colluvial sands form the topping layers. OSL dating yielded Late Pleistocene ages of both lacustrine and eolian sediments ranging from 27.7 ± 2.5 to 17.2 ± 1.4 ka (Table 4).

Section ZAN 1 (~3700 m a.s.l., middle Kyichu Valley, Fig. 1) is located in an inactive sector of the Kyichu floodplain lying about 2–3 m above the present river level. It was accessible due to excavation for brick manufacture. The 3-m-thick exposure consists of a topping portion with fluvial-lacustrine silt and sand, and a basal portion with well-rounded fluvial cobble to granule (Fig. 5). The fluvial–lacustrine deposits are free of $CaCO_3$ and dominantly poor in OC (0.6%; Table 1). They show horizontal bedding (partly lamination) and sometimes contain drop stones in the size of granule (Table 1). The lowermost part between 220 and 250 cm has a high content of OC (7.3%) and bears dispersed wood and charcoal pieces of *Hippophae* giving a ^{14}C age of 7771 ± 70 cal BP (Tables 2,3).

Section CHS 1 (~4040 m a.s.l., side valley of the Kyichu; Fig. 1) exposes the fill of a valley bottom. An upper layer of colluvial sands overlies a sequence of fluvial sands containing paleosols (Figs 5,6a). Both units bear pebbles and cobbles, partly even boulders up to 0.4 m in axis length. The relatively thick topsoil developed from colluvial sand can be assigned to an Arenosol. The layers of fluvial sand are free of $CaCO_3$ and are nearly free of OC (Table 1). They bear signs of both relic (down to ~4.5 m) and present-day (below ~4.5 m) groundwater influence. Three paleosols divide the fluvial sequence, in which the uppermost one

Table 4 Luminescence data

Lab. No.	Sample	Depth [cm]	Cosmic. dose [µGy/y][†]	U[‡] [µg/g]	Th[‡] [µg/g]	K[‡] [%]	Dose rate [Gy/ka]	Water content [%]	ED [Gy]	Age [ka]
										IRSL:
MR0389	QUG1A	25	332 ± 17	6.04 ± 0.30	32.20 ± 1.61	2.36 ± 0.12	9.0 ± 1.0	10 ± 5	3.1 ± 0.6	0.3 ± 0.1
MR0390	QUG1B	73	321 ± 16	5.45 ± 0.27	35.30 ± 1.77	2.42 ± 0.12	9.2 ± 1.0	10 ± 5	7.0 ± 0.6	0.8 ± 0.1
MR0391	QUG1C	115	312 ± 16	4.36 ± 0.22	28.00 ± 1.40	2.85 ± 0.14	8.3 ± 0.8	10 ± 5	8.3 ± 0.5	1.0 ± 0.1
MR0392	QUG1D	122	310 ± 15	5.10 ± 0.26	31.80 ± 1.59	2.72 ± 0.14	8.9 ± 0.9	10 ± 5	71.4 ± 1.3[§]	8.0 ± 0.8
MR0393	QUG1E	153	303 ± 15	3.73 ± 0.19	31.30 ± 1.57	2.51 ± 0.13	8.1 ± 0.8	10 ± 5	162 ± 2.0[§]	20.0 ± 2.0
MR0394	GAR1A	31	328 ± 16	4.71 ± 0.24	29.70 ± 1.49	2.62 ± 0.13	8.4 ± 0.8	10 ± 5	3.6 ± 0.8	0.4 ± 0.1
MR0395	GAR1B	65	320 ± 16	6.06 ± 0.30	35.50 ± 1.78	2.94 ± 0.15	10.0 ± 1.0	10 ± 5	8.7 ± 0.6	0.9 ± 0.1
MR0396	GAR1C	120	308 ± 15	6.23 ± 0.31	40.50 ± 2.03	2.79 ± 0.14	10.5 ± 1.1	10 ± 5	16.7 ± 0.8	1.6 ± 0.2
MR0397	GAR1D	175	296 ± 15	5.74 ± 0.29	40.90 ± 2.05	3.07 ± 0.15	10.6 ± 1.1	10 ± 5	27.6 ± 0.8	2.6 ± 0.3
MR0398	GAR1E	204	290 ± 14	5.36 ± 0.27	33.80 ± 1.69	2.41 ± 0.12	9.0 ± 0.9	10 ± 5	28.1 ± 0.7	3.1 ± 0.3
MR0399	GAR1F	218	288 ± 14	4.90 ± 0.25	32.00 ± 1.60	2.28 ± 0.11	8.4 ± 0.9	10 ± 5	35.8 ± 1.1[§]	4.3 ± 0.5
MR0400	GAR1G	243	283 ± 14	6.22 ± 0.31	42.10 ± 2.11	3.09 ± 0.15	11.0 ± 1.1	10 ± 5	41.1 ± 1.3[§]	3.7 ± 0.4
										OSL:
MR0545	STA1A	50	333 ± 40	2.76 ± 0.19	17.33 ± 1.21	2.72 ± 0.14	4.76 ± 0.36	10 ± 5	14 ± 0.4	2.9 ± 0.2
MR0546	STA1B	180	267 ± 19	2.69 ± 0.18	17.34 ± 1.21	2.68 ± 1.13	4.64 ± 0.36	10 ± 5	19 ± 1.1	4.1 ± 0.4
MR0547	STA1C	280	227 ± 15	3.10 ± 0.22	18.73 ± 1.31	2.65 ± 0.13	4.78 ± 0.37	10 ± 5	32 ± 0.6	6.7 ± 0.5
MR0548	CHI1F	70	320 ± 31	2.66 ± 0.19	18.4 ± 1.29	2.79 ± 0.14	4.86 ± 0.37	10 ± 5	70 ± 4	14.4 ± 1.4
MR0549	CHI1E	300	219 ± 14	2.83 ± 0.20	18.3 ± 1.28	2.86 ± 0.14	4.86 ± 0.38	10 ± 5	96 ± 5	19.8 ± 1.9
MR0550	CHI1C	650	132 ± 9	2.33 ± 0.16	15.28 ± 1.07	2.45 ± 0.12	4.05 ± 0.32	10 ± 5	97 ± 4	23.9 ± 2.1
MR0551	CHI1B	1000	87 ± 6	2.86 ± 0.20	17.21 ± 1.21	2.95 ± 1.15	4.74 ± 0.38	10 ± 5	101 ± 3	21.3 ± 1.8
MR0552	QUX2A	130	284 ± 21	1.92 ± 0.13	11.36 ± 0.79	2.63 ± 0.13	4.01 ± 0.31	10 ± 5	69 ± 2	17.2 ± 1.4
MR0553	QUX2B	600	139 ± 9	2.71 ± 0.19	17.71 ± 1.24	2.67 ± 0.13	4.48 ± 0.34	10 ± 5	73 ± 7	16.3 ± 2.0
MR0554	QUX2C	950	91 ± 6	2.74 ± 0.19	15.5 ± 1.08	2.45 ± 0.12	4.09 ± 0.31	10 ± 5	113 ± 5	27.7 ± 2.5
MR0555	MOG4A	130	304 ± 23	3.45 ± 0.24	22.26 ± 1.56	2.33 ± 0.12	4.93 ± 0.37	10 ± 5	139 ± 11	28.2 ± 3.1
MR0556	MOG4C	350	213 ± 14	2.99 ± 0.21	18.21 ± 1.28	2.29 ± 0.12	4.39 ± 0.34	10 ± 5	354 ± 12	81.0 ± 7.0
MR0557	MOG4E	600	149 ± 10	3.25 ± 0.23	20.62 ± 1.44	2.48 ± 0.12	4.73 ± 0.37	10 ± 5	388 ± 19	82.0 ± 8.0
MR0558	MOG4F	800	116 ± 7	3.15 ± 0.22	16.76 ± 1.17	2.37 ± 0.12	4.29 ± 0.33	10 ± 5	506 ± 29	118.0 ± 11.0
MR0559	GYA3A	160	286 ± 20	3.0 ± 0.21	19.46 ± 1.36	2.31 ± 0.12	4.52 ± 0.34	10 ± 5	154 ± 7	34.1 ± 3.0
MR0560	GYA3B	320	221 ± 15	3.04 ± 0.21	18.58 ± 1.30	2.34 ± 0.12	4.50 ± 0.34	10 ± 5	202 ± 9	44.8 ± 4.0
MR0561	GYA3C	400	195 ± 13	1.92 ± 0.13	11.36 ± 0.80	2.63 ± 0.13	4.45 ± 0.34	10 ± 5	279 ± 24	63.0 ± 7.0
MR0562	DRE18A	330	215 ± 14	3.26 ± 0.23	21.00 ± 1.47	2.44 ± 0.12	4.79 ± 0.37	10 ± 5	155 ± 10	32.3 ± 3.2
MR0563	DRE18B	590	146 ± 9	5.46 ± 0.38	19.55 ± 1.37	1.91 ± 0.09	4.72 ± 0.36	10 ± 5	326 ± 23	69.0 ± 7.0
MR0564	DRE18C	850	105 ± 7	3.59 ± 0.25	21.99 ± 1.54	2.18 ± 0.11	4.61 ± 0.36	10 ± 5	377 ± 19	82.0 ± 8.0

[†] KosmDL v1.0 software (K. D. Karelin, unpubl. data, 2000); [‡] Neutron activation analyses; [§] max. beta dose of 353 Gy.
ED, equivalent dose.
Site information (altitudes, coordinates) is available in Table 1.

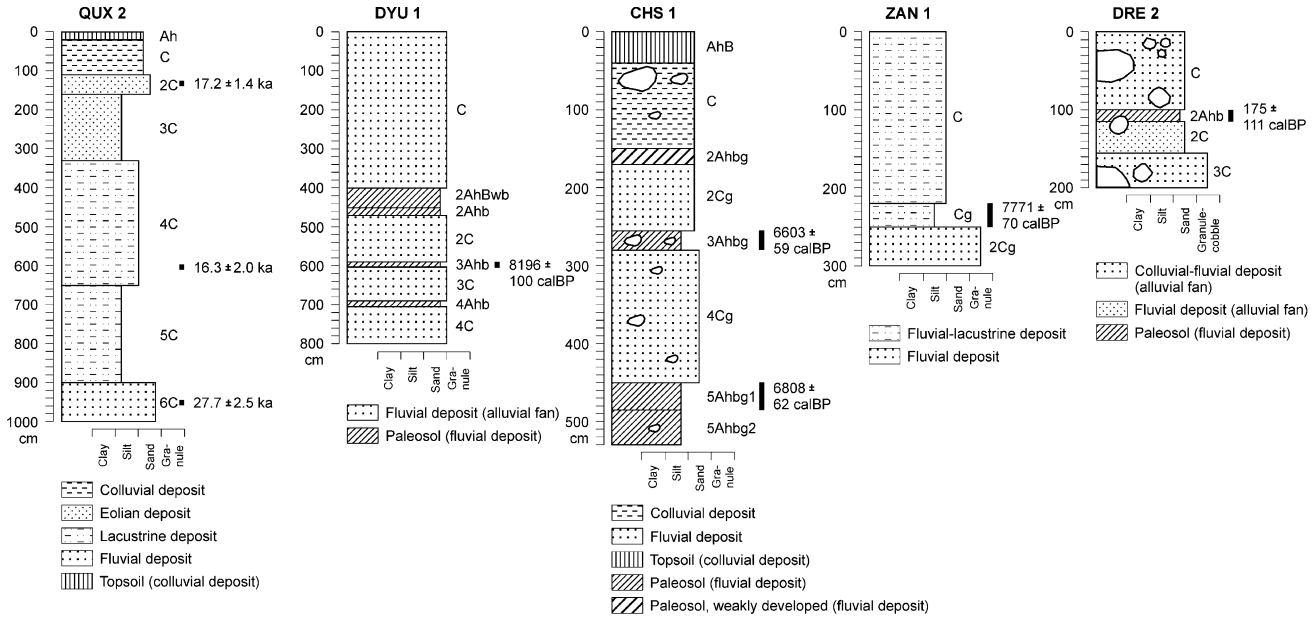

Fig. 5 Logs of the fluvial–lacustrine sequences recorded.

(2Ahbg) is, according to color and OC content (0.6%), a weakly developed relic Gleysol. The lower paleosols (3Ahbg, 5Ahbg) have high contents of OC (4.7–5.5%) and are black and very dark brown in color, respectively. They consist of loams and silts and can be classified as (partly relic) Gleysols. In the lowermost paleosol (below 4.5 m), both the unusually low pH values (decreasing from pH 6.8 to 2.5) and the unusually high EC values (increasing from 0.100 to 3.470 mS/cm) point to changes in the mineralogical composition, possibly comprising a higher content of metal oxides. The charcoal spectrum from the middle paleosol (3Ahbg) is dominated by an indeterminable deciduous wood, which was ^{14}C dated to 6603 ± 59 cal BP (Tables 2,3). Wood fragments occur in the lower paleosol (5Ahbg) consisting exclusively of *Hippophae*, which gave a ^{14}C age of 6808 ± 62 cal BP.

Section DRE 2 (~3650 m a.s.l., northwestern margin of the Lhasa Basin; Fig. 1) represents a 2-m-thick cliff section of a gully lying on the middle portion of a widely inactive alluvial fan below a steep mountain ridge. The profile consists of a topping layer of coarse fan sediment, an intermediate layer of fluvial sand including paleosol, and a basal layer of coarse fan sediment (Fig. 5, Table 1). The fine matter of the layers analyzed is badly sorted loamy and silty sand. The upper layer contains well-rounded cobbles and boulders of granite with a maximum axis length of 1.4 m. The 0.15-m-thick paleosol (2Ahb horizon) is developed from fluvial sand having distinct enrichment of organic matter (LOI = 4.0%). It contains a broad spectrum of artifacts (pot shards, bone chips, charcoal). Charcoal analysis shows a dominance of *Juniperus* (54.6%) followed by a high portion of *Salix* (38.1%; Table 2). A ^{14}C sample of *Juniperus* charcoal yielded a (subrecent) age of 175 ± 111 cal BP (Table 3). The paleosol is assigned to an Arenosol. The basal layer of fan sediment is dominated by coarse matter (90%) consisting of granules to boulders with a maximum axis length of 1.8 m.

Section DYU 1 (~3700 m a.s.l., side valley of the Tolungchu; Fig. 1) was recorded in a sand quarry lying on a small inactive alluvial fan. The 8-m-thick exposure consists of coarse-grained fluvial sands, which derive from short-distance transport from the adjacent steep mountain ridge of granite (Fig. 5). The fluvial sands bear a distinct amount of fine-grained granules (10–40%) and have no detectable organic or carbonate content. Three paleosols occur in the lower part of the section (2Ahb, 3Ahb, 4Ahb) having a very small OC content (0.2–0.4%; Table 1). They were classified as Arenosols. Charcoal from the middle paleosol (3Ahb) was determined as *Sophora* yielding a ^{14}C age of 8196 ± 100 cal BP (Tables 2,3).

EOLIAN SEQUENCES

The eolian sequences presented in this study consists of: (i) loesses (MOG 4, GYA 3); and (ii) eolian sands (CHI 1, STA 1). In general, loess can be defined simply as a terrestrial clastic sediment,

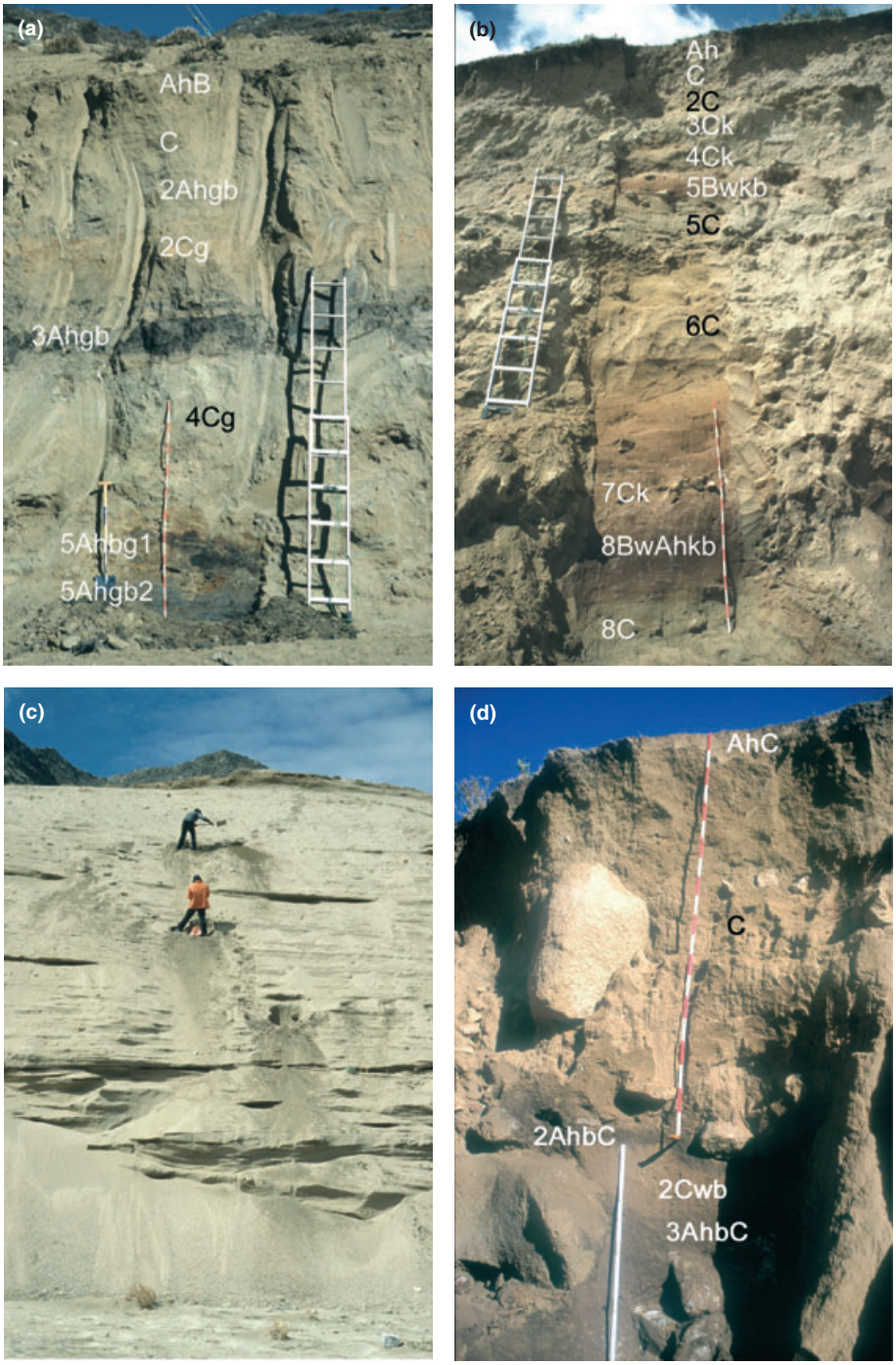

Fig. 6 Photographs of selected sections investigated, (a) section CHS 1 predominately consisting of fluvial sediments with paleosols (~4040 m a.s.l., length of the ruler = 200 cm), (b) section MOG 4 predominately consisting of silty and sandy eolian sediments with paleosols (~3890 m a.s.l., length of the ruler = 200 cm), (c) Section CHI 1 predominately consisting of eolian sands (~3620 m a.s.l.), (d) section GAR 1 predominately consisting of colluvial sands with paleosols (~3800 m a.s.l., length of the upper ruler = 200 cm).

composed predominantly of silt-size particles and formed essentially by the accumulation of wind-blown dust (Pye 1995).

Section MOG 4 (~3890 m a.s.l., valley flank of the Madromachu; Fig. 1) is located on a footslope, which was exposed by extraction of raw material. The dominant portion of the 9-m-thick sequence consists of eolian sediments (silts, loams, silty sands; Figs 6b,7, Table 1). Intercalated thin layers and the top consist of colluvial sands and silts having a content of coarse matter (granules to boulders) up to 20%. Two paleosols occur in the

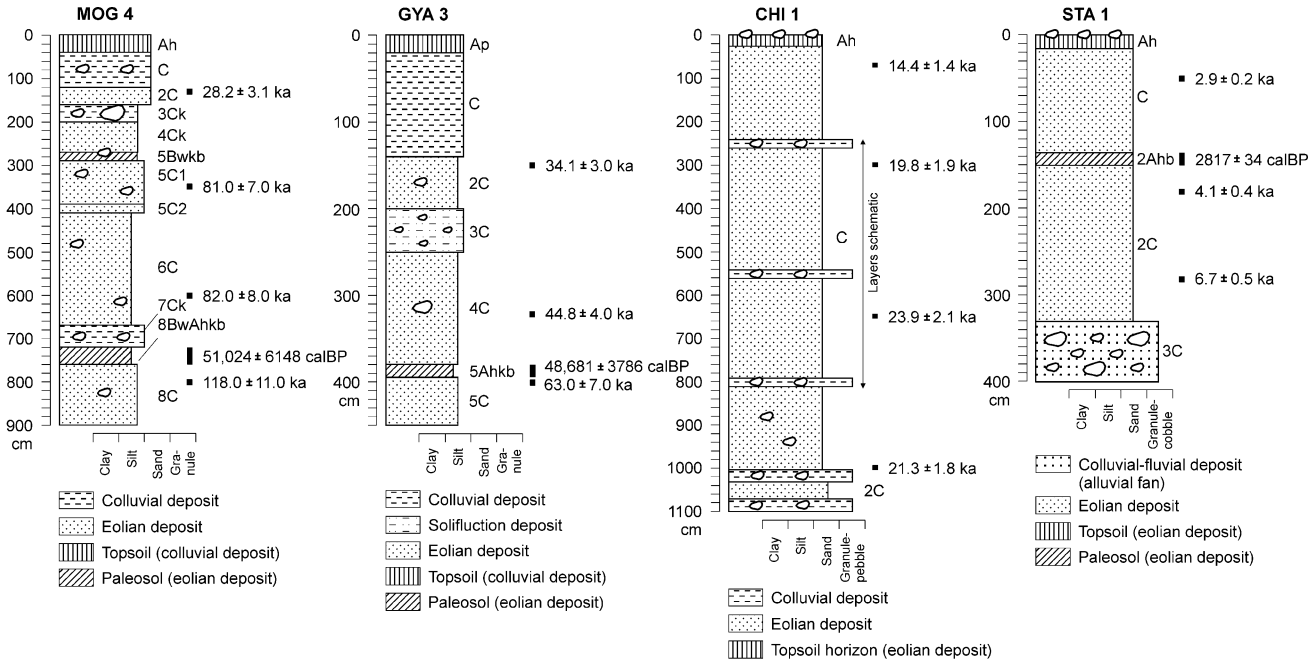

Fig. 7 Logs of the eolian sequences recorded.

eolian sediments. The 0.2-m-thick upper paleosol (5Bwkb) is characterized by a yellowish brown color and very low OC content. It is classified as a Calcaric Cambisol (-remain). The lower 0.4-m-thick 8BwAhkb horizon has a relatively low OC content (0.4%) but a striking chestnut brown color. According to the color, the enrichment of secondary carbonate and the well-developed mollic structure, this paleosol can be classified as a Kastanozem. In this horizon small and smeary charcoal pieces occur. The spectrum consists of *Caragana*, *Hippophae*, and an indeterminate deciduous wood yielding a ^{14}C age of 51 024 ± 6148 cal BP (Tables 2,3). OSL dating of the eolian silts about 0.5 m below gave an age of 118.0 ± 11.0 ka, whereas samples from the overlying eolian layers yielded OSL ages from 82.0 ± 8.0 to 28.2 ± 3.1 ka (Table 4).

Section GYA 3 (~3840 m a.s.l., valley flank of a tributary stream of the Kyichu, Fig. 1) exposes a footslope sequence cut by the extraction of raw material. The 4.5-m-thick section is formed by a topping colluvial layer (silt), originating from hillwash, and subsequent loess layers (Fig. 7). In the upper part of the loess section, a thin colluvial bed consisting of silt and granule to cobble occurs, which is interpreted as a solifluction deposit. In the lower portion, there is an only 0.15-m-thick paleosol developed from loess (5Ahkb, OC = 0.5%, $CaCO_3$ = 1.1%; Table 1), which is classified as Regosol. Charcoal, determined as Rosaceae/Maloideae, yielded a ^{14}C age of 48 681 ± 3786 cal BP (Tables 2, 3). An OSL sample of loess directly below yielded 63.0 ± 7.0 ka. Loess layers above the paleosol date 44.8 ± 4.0 and 34.1 ± 3.0 ka (Table 4).

Section CHI 1 (~3620 m a.s.l., valley flank of the Kyichu; Fig. 1) was recorded in a gully which cuts an active eolian sand area (~2 km × 1 km). The eolian sands cover the distal part of the (former) Kyichu floodplain and climb up the valley flank reaching about 4200 m a.s.l. Between the active river and the eolian sand area, there is a strip of irrigated arable land and woodlands forming a barrier of *potential* eolian sand transport from the river to the slope (Fig. 3c). The 11-m-thick section is divided in a sandy eolian upper part (0–10 m) having a few thin layers of colluvial granule and pebble, and a lower part (10–11 m) consisting of alternating sandy eolian and colluvial layers (Figs 6c,7). The whole section is well-layered, showing parallel bedding that follows the weak inclination of the slope. The eolian sands are dominated by the fine fraction. A higher silt portion occurs in the uppermost part (0–1 m, 46–47%; Table 1). There is no clear discontinuity of the eolian sedimentation, such as a paleosol, except the colluvial layers mentioned. OSL dating yielded for the thick sequence four ages between 23.9 ± 1.8 and 14.4 ± 1.4 ka (Table 4).

Section STA 1 (~3660 m a.s.l., valley flank of the Kyichu; Fig. 1) is situated on an alluvial fan next to a mountain footslope. The 4-m-thick sequence is exposed by a gully which dissects the inactive fan. Two layers of eolian (fine) sand overlay gravelly fan deposit (Fig. 7). The separating brownish paleosol (2Ahb) has a distinct OC content (0.7%) and is classified as Arenosol. A charcoal spectrum from this paleosol is dominated by *Juniperus* yielding a ^{14}C age of 2817 ± 34 cal BP (Tables 2,3). OSL ages from the eolian sands range from 6.7 ± 0.5 to 2.9 ± 0.2 ka (Table 4).

COLLUVIAL SEQUENCES

Generally, colluvial sediments are represented by several badly sorted deposits whose transport and sedimentation took place gravitationally in a water-supported setting. The transport was often over a short distance. However, the term 'colluvial' bears the potential for profound misunderstanding (Kleber 2006). The British 'colluvium' is less strictly defined. In the United States, 'colluvium' often refers to mass-wasting deposits upon slopes in contrast to 'alluvium', which is attributed to running water. Some definitions include all slope deposits, that were driven by gravitation or by unconcentrated runoff, whereas others restrict the occurrence to footslopes excluding fluvial processes or including the latter. Finally, the German term 'Kolluvium' is in its narrowest sense defined as a deposit created on slopes by running water due to *human-induced* soil erosion (Leopold & Völkel 2007). In this study, we use a less strict definition: even badly sorted sediments on slopes and alluvial fans are considered to be 'colluvial'.

The sequences presented can be divided into: (i) a complexly composed alluvial fan section bearing colluvial, fluvial, and eolian deposits (DRE 18); and (ii) footslope sections consisting of hillwash plus rockfall (GAR 1, QUG 1).

Section DRE 18 (~3710 m a.s.l., northwestern margin of the Lhasa Basin; Fig. 1) is located on the topographically upper part of the Drepung alluvial fan, which was already mentioned above in connection with the presentation of section DRE 2. The section was recorded in a 13-m-deep gully (Fig. 3e). It is composed of several sediments, being colluvial (prevailing on top and at the base), fluvial (on top), and eolian (mid position; Fig. 8). The colluvial layers consist of sands with some granules to cobbles having nearly no OC and only low $CaCO_3$ content. The fluvial layer consists of granules. Silts and silty sands form the eolian layers, which bear low organic (0.2–0.3%) but sometimes considerable $CaCO_3$ contents (5.1–15.5%; Table 1). Two incipiently developed paleosols occur in the eolian layers having low OC (0.2–0.4%), but rather high $CaCO_3$ values (3.9–16.8%). The soil colors are brownish. Obvious humic particles, such as charcoal, are lacking. Both paleosols can be classified as (relics of) Calcaric Cambisols. The age of the mainly eolian sediments between 300 and 900 cm is revealed by three OSL ages comprising 32.3 ± 3.2 to 82.0 ± 8.0 ka (Table 4). In the topsoil, a well-preserved human skeleton (60–80 cm, intentional grave?) was found yielding a radiocarbon age on bone of 2272 ± 68 cal BP (Table 3).

Section GAR 1 (~3800 m a.s.l., Tolungchu Valley; Fig. 1) is situated on the footslope of a mountain ridge consisting of granite, which is a few hundred meters high (Fig. 3f). It comprises a succession of different colluvial layers of loamy sand overlying a fluvial–lacustrine sand layer (Figs 6d,8). The upper colluvial layer is 2 m thick and contains a higher proportion of dispersed coarse matter such as pebbles and boulders of granite up to a size of 0.8 m × 0.4 m. Site position and structural–textural properties point to a sediment formation by a combined colluvial process of hillwash plus rockfall. The upper paleosol (2AhbC horizon), developed from colluvial sand (Table 1), represents an occupation layer. Pot shards, lithic artifacts, bones, and charcoal as well as some metal objects such as slag have been detected in this horizon. Typologically, the pot shards represent the Late Neolithic period (Kaiser *et al.* 2006). A large quantity of coarse and fine charcoal pieces has caused a marked black coloration and a relatively high level of LOI (5.8%). Shrubs dominate the charcoal spectrum (*Hippophae* 70.5%, *Rosa* 23.3%; Table 2); only a small portion is represented by *Juniperus* (5.4%). The ^{14}C dating on *Juniperus* charcoal from the upper paleosol yielded an age of 4005 ± 79 cal BP (Table 3). IRSL age estimates obtained for the upper 2.5 m of the profile point to a successive deposition of the colluvial sands within the last 4.3 ± 0.5 ka (Table 4). The dark color and the accumulated thickness (95 cm) of the lower paleosol (3AhbC and 3Ah/Bwb horizons) are remarkable. Typologically, it is classified as a Phaeozem. This paleosol yielded a ^{14}C age of 8781 ± 152 cal BP on bulk soil matter. The basal layer, having a relatively large amount of clay (18%) and nearly 14% of $CaCO_3$, is interpreted to be of fluvial–lacustrine origin.

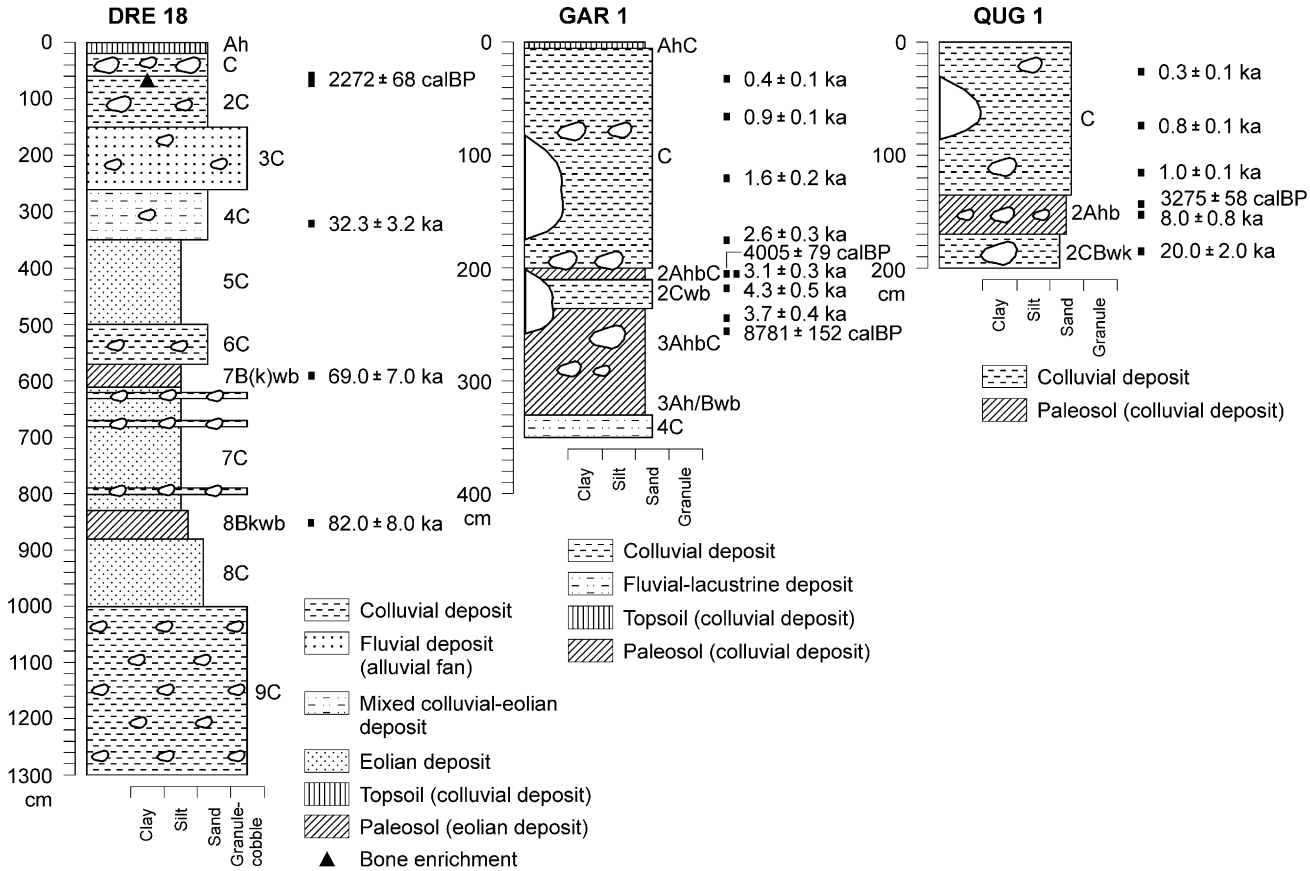

Fig. 8 Logs of the colluvial sequences recorded.

Section QUG 1 (Neolithic Qugong site, ~3680 m a.s.l., northern margin of the Lhasa Basin; Fig. 1) is located at a hill footslope, which is a few tens of meters high and mostly exposing barren granite. Bedrock outcrops only 10 m above the profile. This is the second major Neolithic site found on the Tibetan Plateau (after Karou site, Chamdo, eastern Tibet), dating *ca* 1050–1750 BC (= *ca* 3000–3700 cal BP). It was excavated in the early 1990s (Institute of Archaeology of the Chinese Academy of Social Sciences and the Bureau of Cultural Relics of the Tibet Autonomous Region 1999; Aldenderfer & Zhang 2004; Aldenderfer 2007). QUG 1 forms a 2-m-thick sequence of a topping colluvial layer and a buried paleosol-bearing colluvial deposit (Fig. 8). All layers consist of loamy sand. The upper colluvial layer bears some boulders of 1.5 m maximum axis length, indicating sediment formation by a combined colluvial process of hillwash plus rockfall. Due to the lack of a humic topsoil horizon (Ah), this layer was probably subjected to some post-depositional erosion. A 0.35-m-thick buried paleosol (2Ahb) represents the occupation layer. This greyish brown horizon (LOI = 2.5%) contains a large quantity of burned and broken granules and pebbles, pot shards, bones, and flakes. Pedological properties assign this paleosol to an Arenosol. One radiocarbon sample of animal bone was taken from the 2Ahb horizon and yielded an age of 3275 ± 58 cal BP (Table 3). Only some very small and smeary pieces of charcoal were found, not allowing extraction from the paleosol and further analysis. However, a comparable section was recorded a few tens of meters to the northwest yielding in the paleosol a *Hippophae*-dominated charcoal spectrum (Table 2). IRSL ages indicate an accumulation of the overlying colluvial layer within the last thousand years (Table 4). Two samples from the underlying colluvial deposits yielded ages of 8.0 ± 0.8 and 20.0 ± 2.0 ka.

DISCUSSION

RELIABILITY OF GEOCHRONOLOGICAL DATING

The reliability of polymineral fine grain IRSL ages has already been discussed in Kaiser *et al.* (2006),

and the IRSL ages are generally in agreement with the ^{14}C ages where available. For quartz OSL ages, the normal distribution of equivalent doses within a sample (>12 aliquots) determined by the SAR protocol shows that the sample has been well-bleached before deposition. The conditions adopted for the SAR protocol are verified by the successful laboratory dose recovery test.

The four luminescence ages of >80 ka in sections MOG 4 and DRE 18 should be regarded as minimum ages because equivalent doses are approaching the saturation level in the growth curve of quartz OSL. However, in terms of paleoenvironmental interpretation, these OSL ages are in stratigraphic order and are still meaningful. In section MOG 4, ^{14}C dating on charcoal from the paleosol at the lower part of the section yielded an age of 51 024 ± 6148 cal BP. At first glance this suggests that it might have been formed during Marine Isotopic Stage (MIS) 3. However, the three OSL ages of >80 ka indicate that this paleosol was probably formed during the Last Interglacial. Considering the OSL ages available, and bearing in mind the limits of radiocarbon dating, this ^{14}C dating should be regarded as a minimum age only, as it might have been rejuvenated by contamination with younger carbon. The geochronological dating results of all other sections seem to be reliable, taking into account the IRSL and OSL data, the chronological control by ^{14}C ages, and the stratigraphic order of the data per section.

FLUVIAL–LACUSTRINE DYNAMICS

On the one hand, there is a conspicuous lack of (high-lying) fluvial or lacustrine terraces in the Kyichu Valley downstream from Maizhokungar. On the other hand, only a few sections directly from the floodplains of the river and its tributaries are available due to the rarity of suitable exposures. Thus, information on the regional fluvial–lacustrine dynamics based on this study is very restricted.

Fluvial–lacustrine deposits of both Late Pleistocene (QUX 2) and Holocene (DYU 1, CHS 1, ZAN 1, DRE 2) ages were detected. In cases where a multi-level dating of a section is available, partly high sedimentation rates become apparent (QUX 2, CHS 1). Downstream the Yarlung Zhangbo, high-lying fluvial–lacustrine sediments comparable with section QUX 2 exist, both in the vicinity of QUX 2 (southwest of Gongar Airport, ~10 km away) and at several sites up to approximately 65 km eastward (south of Samye Monastery; Fig. 1). They form heavily dissected terraces lying 10–20 m above the present floodplain. Zhang (1998) has supposed a Late Pleistocene age considering the ^{14}C dating of a lacustrine 15-m-terrace a few tens of kilometers upstream of Quxu (37 000 ± 6000 BP on wood ≈ 41 000 ± 6000 cal BP). Possibly, all occurrences reflect the sedimentation in the same Late Pleistocene dam-lake filling up this section of the Yarlung Zhangbo Valley and the mouth areas of its tributaries. In general, the morphological structure of this valley comprising alternating sections of wide basin-like parts and narrow gorges favors the formation of damming bodies following tectonic, glacial, and landslide events (Zhang 1998, 2001; Montgomery *et al.* 2004). Thus, during the very Late Pleistocene, the mouth area of the Kyichu was occupied by a lake depositing lacustrine silts, whose drying-up is proven by overlying eolian deposits dating around 17.2 ± 1.4 ka.

The absence of fluvial–lacustrine terraces above the present floodplain in the middle and lower course of the Kyichu, opposite to well preserved terraces existing upstream of Maizhokungar, can be explained only tentatively. Even in the adjoining section of the Yarlung Zhangbo Valley, no terrace higher than 25 m and older than the Late Pleistocene has been found (Zhang 1998). It is known from geophysical research that the Quaternary valley fill of the Lhasa Basin reaches a thickness of nearly 500 m (Zhang 1998; Shen *et al.* 2007) pointing to the aggradational character of the valley fill. Accordingly, alluvial sediments could bury not only older valley bottoms but also possibly existing older terraces. Another but less probable explanation concerns a complete removal of formerly existing high-lying structures by fluvial erosion.

In general, valley formation and corresponding environmental changes in that area seem to have been profoundly affected by neotectonic movements. Probable block movements of valley sections could have caused specific geomorphic effects (e.g. blockade of fluvial drainage and formation of dam-lakes) and give rise to difficulties for the topographical correlation between landforms and sediments (Zhang 1998, 2001).

EOLIAN DYNAMICS

Nearly the whole study area is covered with a mostly thin veneer of eolian sediments except active fluvial and peat bog sites, screes, or barren rocks. Only locally (particularly on footslope posi-

tions and in eolian sand areas) does the thickness of loess or eolian sand exceed 5 m.

Most of the sections presented reveal Last Glacial/Late Pleistocene eolian sediments (MOG 4, GYA 3, CHI 1) spanning OSL age estimates from 118.0 ± 11.0 to 14.4 ± 1.4 ka. In contrast, only one eolian sequence was assigned to the Late Holocene (STA 1). Considering the dating from loess alone, the ages span a time interval from 118.0 ± 11.0 to 28.2 ± 3.1 ka suggesting a dominant genesis *before* the Last Glacial Maximum (LGM). Thus, our loess dating results contradict the generalized conclusion of Sun *et al.* (2007), who supposed that the present loess in southern/interior Tibet has accumulated since the last deglaciation, suggesting a lack of full-glacial loess. The Pleistocene eolian sands, on the other hand, exclusively show Late Pleistocene ages ranging from 23.9 ± 2.1 to 14.4 ± 1.4 ka suggesting a dominant genesis around and particularly *after* the LGM.

Both the loess and the eolian sand ages represent the oldest datings of eolian sediments from southern and interior Tibet available so far. This can be deduced by means of a recently established database of luminescence ages (OSL, IRSL, TL) pertaining to the whole plateau, which comprises about 150 datings (Kaiser 2007). According to ^{14}C-dated paleosols developed from loess, which are mostly overlain by loess as well, distinct eolian phases have occurred during the Late-glacial and the Late Holocene. In contrast, there are only few luminescence dates from eolian sands showing Late-glacial and Holocene ages (Klinge & Lehmkuhl 2003; Kaiser 2007). However, ^{14}C datings on paleosols developed on and overlain by eolian sands prove that there have been locally eolian phases throughout the Late-glacial–Holocene period (e.g. Li *et al.* 2006; Porter & Zhou 2006).

According to an investigation of loesses in the adjacent middle reach of the Yarlung Zhangbo Valley, geochemical, mineralogical, and granulometrical evidence indicate a *local* provenance of loess in southern Tibet resulting from eolian sorting of glaciofluvial and fluvial deposits (Sun *et al.* 2007).

In contrast to the Yarlung Zhangbo Valley, where vast active dune and coversand fields climb to maximum elevations of nearly 2000 m above the present floodplain (Liu & Zhao 2001; Sun *et al.* 2007; Switzer *et al.* 2007), areas in the Kyichu Valley consisting of eolian sand are less expanded. Evidently, if active, they have been reactivated by human impact during the Late (?) Holocene (see below).

PALEOSOL OCCURRENCES

Generally, a paleosol represents an interruption or deceleration of sedimentation, indicating a stabilization of the geomorphic system. The burial of a paleosol, on the other hand, represents an activation of the geomorphic system, which requires both local sediment accumulation and extra-local erosion. In contrast to the adjacent Chinese Loess Plateau (e.g. An *et al.* 2006; Feng *et al.* 2006), knowledge of Late Quaternary paleopedology on the Tibetan Plateau and its use for paleoenvironmental interpretation are still in their infancy (e.g. Fang *et al.* 2003; Kaiser *et al.* 2007).

Paleosols regularly occur at terrestrial ('dry') sites of the study area. Nine of the 12 sections presented bear paleosols; some of the sections have two paleosol layers or more. All paleosols bear macroscopic charcoal allowing extraction for botanical determination and accordant paleoenvironmental interpretation (see below) as well as for ^{14}C dating.

Several terrestrial soil types have been detected (e.g. Phaeozems, Kastanozems, Calcaric Cambisols, Arenosols, Regosols), which, in general and regardless of their large age span, comprising probably the Last Interglacial to the very Late Holocene, represent soils of temperate to cool and humid to semiarid site conditions. However, mostly less differentiated and, with respect to their environmental indicator value, rather uncharacteristic Arenosols were predominantly detected. They have carbonate-free Ah horizons with low thicknesses (10–35 cm) and contain relatively small organic contents only (OC = 0.2–0.7%, LOI = 2.5–4.0%). In terms of pedogenesis, the most noticeable paleosols recorded are a 40-cm-thick BwAhkb horizon of probable Last Interglacial age (MOG 4, ~3890 m a.s.l., Kastanozem) and a 75-cm-thick AhbC horizon of Early Holocene age (GAR 1, ~3800 m a.s.l., Phaeozem). As far it is known, modern terrestrial soils of comparable altitudes in the Lhasa region do not have such well-developed appearances, which might be caused by Late Holocene climate changes and/or by Late Holocene erosional processes. In particular the buried Phaeozem of section GAR 1, whose development required a denser vegetation and a higher moisture than presently occurring at this site (grazed very sparse grass cover, MAP = 400–500 mm), clearly indicates Holocene environmental changes. Similar pedogenic successions from 'wet' to 'dry' features have been described from Mid- to Late Holocene sections of central and

eastern Tibet (Lehmkuhl *et al.* 2002; Klinge & Lehmkuhl 2003). All records might represent an aridification, corroborating the conclusions of Lehmkuhl and Haselein (2000), Tang *et al.* (2000) & Herzschuh (2006), for example, on the climatic tendency of the Tibetan Plateau in that time span to be cool and dry.

For the first time in southern Tibet, paleosols older than the Holocene were detected. Besides a probable Last Interglacial Kastanozem (MOG 4) and two early Last Glacial Calcaric Cambisols (DRE 18, MIS 4–5c/d), a Regosol dating from MIS 3 (GYA 3) was found. Including a further ^{14}C age from an alluvial fan deposit (MAR 1, ~3890 m a.s.l., 34 247 ± 619 cal BP, *Caragana* charcoal, Erl-10121), these ages indicate ice-free valley grounds during MIS 4–5c/d to 3 comprising a well developed and vegetated soil cover. This finding corresponds to conclusions made by Shi *et al.* (2001), who suggest, after reviewing several geological records (ice cores, lake sediments, pollen diagrams), that on the plateau the period 30 000–40 000 BP (= *ca* 34 000–44 000 cal BP) was distinctly warmer and moister than today (MAAT = 2–4°C higher, MAP = 40–100% higher).

Moreover, in the altitude studied (~3600–4000 m a.s.l.) no glacial relics, which might for example be represented by moraines, tills, or striated erratics, were found, indicating that at least the valley positions in the study area have been free of glaciers since the Last Interglacial.

COLLUVIAL PROCESSES, VEGETATION CHANGES AND HUMAN IMPACT

In the study area, colluvial sediments of both Late Pleistocene age (<82.0 ± 8.0–20.0 ± 2.0 ka) and Late Holocene age (4.3 ± 0.5–0.3 ± 0.1 ka) were detected. Regarding their subfacies, these deposits can be divided into: (i) coarse-grained sediments with a high proportion of cobbles and boulders originating from alluvial fans (DRE 2, DRE 18); (ii) matrix-supported sediments with only some cobbles and boulders originating from combined colluvial processes of hillwash plus rockfall (QUG 1, GAR 1); and (iii) (periglacial) solifluction deposits (partly GYA 3). Further facies (not presented here) comprise: (iv) more or less fine-grained sediments originating from hillwash (Kaiser *et al.* 2006); and (v) fine-grained sediments originating from intentional anthropogenic accumulation by construction of field terraces (Kaiser 2007).

Large portions of the valley flanks along the Kyichu and Tolungchu consist of barren rock (mostly granite) having a 'desert-like' appearance. However, according to climatic and botanical data, this area presently has a *potential* 'forest climate' (Miehe *et al.* 2006, 2008) allowing the growth of trees, shrubs and a luxuriant cover of herbs and grasses, if it would not be influenced by heavy grazing pressure of domestic animals and by fuel wood extraction (see 'Study area'). Consequently, questions arise by which processes and when were the slopes exposed. Miehe *et al.* (2003) suggest a model on the 'hypothetical desertification process on lower sunny slopes around Lhasa' showing an exposure of slopes in the course of substantial soil erosion following a Late Holocene human-induced vegetation change from a mixed open juniper forest to an anthropic semi-desert. This hypothesis is seemingly corroborated by the results from the GAR 1 and QUG 1 sections showing both Late Holocene colluvial deposits proximately below barren valley slopes, and a clear difference between the vegetation cover before and after the colluvial sedimentation (forest/woodlands according to charcoal determination in the past *vs* sparse grassland at present). However, according to section DRE 18, the up to 15-m-thick colluvial sequences from footslope positions of the Lhasa–Drepung area predominantly date into the Late Pleistocene referring to a widely natural exposition for slope erosion in the far past. By contrast, the relatively thick fluvial deposits of section DYU 1 result from nearby erosion of a small (now exposing barren granite) slope catchment during the Holocene. Thus, it is hypothesized that the barren valley slopes along the Kyichu and Tolungchu were *primarily* formed by a Late Pleistocene erosion phase (probably triggered by ice-age climatic effects) followed by a secondary (probably human-induced) Holocene erosion phase.

The charcoal and fossil wood spectra analyzed partly give clear evidence for Late Quaternary vegetation changes in the study area. The Holocene spectra show distinct differences concerning the past and present vegetation both at dry sites (DRE 2, GAR 1, QUG 1, STA 1) and at wet sites (ZAN 1, CHS 1). The past vegetation is characterized by predominant tree and shrub species (dry sites e.g. *Juniperus*, *Betula*, *Buddleja*; wet sites e.g. *Salix*, *Populus*, *Hippophae*), whereas the present plant cover consists of sparse grasses, herbs, and dwarf shrubs, but even non-vegetated barren fine soil, granule to boulder, and rock occur at a large scale (addition-

ally see pollen diagram 'Lhasa 1/PDL 1' in Miehe *et al.* 2006; Fig. 1). The Late Pleistocene charcoal spectra, by contrast, are rather uncharacteristic, mostly showing shrubs (e.g. *Caragana*, *Sophora*, *Hippophae*), which also presently occur in the area. However, the detection of shrubs does not necessarily indicate a treeless landscape, as they also could represent plant species of the understory occurring in forests and woodlands (e.g. *Sophora moorcroftiana* is growing in Cupressaceae forests of southern Tibet; Miehe *et al.* 2006, 2008).

In the study area, probable past human impact can be deduced from the formation and reactivation of eolian sand areas, the occurrence of relatively young colluvial deposits, and the detection of Late Holocene vegetation changes. The human impact may consist in forest clearing, soil erosion, and land degradation (e.g. following cultivation), construction of field terraces and settlements, irrigation, and grazing. The active eolian sands around section CHI 1 probably represent a subrecently (?) eroded area concluded from the Late Pleistocene dating of the eolian sequence as well as the present lack of sand transport from the potential deflation area, the Kyichu floodplain (vegetation barrier between river and eolian sand field). Even the eolian burying of a formerly forested land surface in section STA 1 (record of juniper) could be caused by human-induced erosion. Furthermore, natural (e.g. exceptional rainfalls, climatic changes) and anthropogenic causes (e.g. slope instability after forest clearing) can be claimed for the formation of the Late Holocene colluvial sediments detected. Also, a combination of both causes (secondary human enhancement of a primary opening of the landscape by increasing aridity and/or coolness as deduced, for instance, from the pollen diagram 'Hidden Lake', Tang *et al.* 2000; Fig. 1) is imaginable. In contrast, the genesis of coarse-grained colluvial sediments with a high proportion of cobbles and boulders originating from alluvial fans can be claimed to support widely natural processes lasting to date. However, human impact can enforce both frequency and magnitude of these events. The genesis of matrix-supported colluvial sediments containing cobbles and boulders, originating from hillwash plus rockfall, as well as that of fine-grained sediments originating from hillwash alone might be caused by human-induced erosion following clearing of forests/woodlands and increased grazing. As the prehistoric presence of humans in the Lhasa region has been confirmed since the Late Neolithic (e.g. Chayet 1994; Aldenderfer & Zhang 2004; Kaiser 2007), it is assumed that the Late Holocene environmental changes, such as loss of forests/woodlands and erosion, at least have been reinforced by humans, emphasizing previous results (Kaiser *et al.* 2006; Miehe *et al.* 2006, 2008).

CONCLUSIONS

The present multidisciplinary study comprising the record of 12 sedimentary sections with subsequent analysis of sediments, paleosols, geochronological samples, and charcoals, conducted along the middle and lower reach of the Kyichu and its tributaries, arrives at the following conclusions:

1. At the altitude studied (~3600–4000 m a.s.l.), no glacial relics could be detected, indicating that the valley positions have been free of glaciers since the Last Interglacial.
2. There is a wide lack of high-lying fluvial or lacustrine structures in the middle and lower Kyichu Valley, which is explained by its aggradational character in a tectonically (sub-) active setting permanently burying older valley bottoms by alluvial sedimentation.
3. During the Late Pleistocene, the mouth area of the Kyichu was occupied by a lake, which fell dry around 17.2 ± 1.4 ka. This (dam-) lake occupied a larger territory in the superordinate Yarlung Zhangbo Valley, affecting even the lower reaches of its tributaries.
4. Outside the active floodplains, the valley surfaces are covered with a mostly thin veneer of eolian silts (loesses) and sands exceeding locally only a thickness of 5 m. OSL ages from loess span a time interval from 118.0 ± 11.0 to 28.2 ± 3.1 ka, suggesting a dominant genesis before the LGM. OSL datings of eolian sands comprise both Late Pleistocene ages (23.9 ± 2.1–14.4 ± 1.4 ka), which suggest a genesis around and after LGM, and Late Holocene ages (6.7 ± 0.5–2.9 ± 0.2 ka).
5. Paleosols of Last Interglacial, Last Glacial, and Holocene ages regularly occur at terrestrial sites, buried by eolian, colluvial, and fluvial sediments. The soil types detected represent temperate to cool and humid to semiarid conditions during soil formation.
6. According to the analysis of colluvial sediments comprising different subfacies, the widespread barren valley slopes along the Kyichu and Tolungchu were primarily formed by Late

Pleistocene erosion, then followed by a secondary (probably human-induced) Holocene erosion phase.
7. The charcoal and fossil wood spectra analyzed give evidence for a Late Holocene change from a tree- and shrub-dominated vegetation to the present plant cover consisting of sparse grasses, herbs, and dwarf shrubs.
8. As the prehistoric presence of humans in the study area has been confirmed since the Late Neolithic, it is assumed that the Late Holocene environmental changes (such as loss of forests/woodlands and erosion) have at least been reinforced by humans, enhancing a climatic aridification and cooling trend.

ACKNOWLEDGEMENTS

We are grateful to Gen Dun, Tibet Museum Lhasa, whose knowledge in regional archaeology enabled us to investigate the sites Qugong and Gar Drongy. The sections of both sites were sampled with the friendly support of La Duo, Lhasa University. Stefan Reiss, Marburg University, assisted with soil analyses. We are indebted to Anja Zander, ASA Laboratory for Archaeometry Wadgassen, for producing the IRSL ages. We thank Tetsuya Sakai, Shimane University for helpful comments on the manuscript, and James Fanning, Greifswald University, for improving the English. We also thank Christiane Enderle, Marburg University, for preparation of Figure 2. Research as well as prints of the color figures were kindly supported by the German Research Foundation (DFG KA 2713/1-1). Zhongping Lai is indebted to the German Alexander von Humboldt Foundation for a fellowship allowing OSL research in the Marburg Luminescence Laboratory.

REFERENCES

AITCHISON J. C., ALI J. R. & DAVIS A. M. 2007. When and where did India and Asia collide? *Journal of Geophysical Research* **112**, B05423.

ALDENDERFER M. 2007. Modeling the Neolithic on the Tibetan Plateau. *Developments in Quaternary Sciences* **9**, 151–65.

ALDENDERFER M. & ZHANG Y.-N. 2004. The prehistory of the Tibetan Plateau to the seventh century A.D.: Perspectives and research from China and the West since 1950. *Journal of World Prehistory* **18**, 1–55.

AN C.-B., FENG Z.-D. & BARTON L. 2006. Dry or humid? Mid-Holocene humidity changes in arid and semi-arid China. *Quaternary Science Reviews* **25**, 351–61.

BÖHNER J. & LEHMKUHL F. 2005. Environmental change modelling for Central and High Asia: Pleistocene, present and future scenarios. *Boreas* **34**, 220–31.

BØTTER-JENSEN L., BULUR E., DULLER G. A. T. & MURRY A. S. 2000. Advances in luminescence instrumentation. *Radiation Measurements* **32**, 523–8.

BRÄUNING A. 2007. Dendroecological studies on the Tibetan Plateau. Implications of relict juniper forests for climate change and cultural history. *Geographische Rundschau International Edition* **3**, 38–43.

CHAYET A. 1994. *Art et Archéologie du Tibet*. Picard, Paris.

CHINESE ACADEMIC EXPEDITION GROUP. 1983. *Geomorphology of Xizang (Tibet)*. Academic Press, Beijing (in Chinese).

CUI X.-F., GRAF H. F., LANGMANN B., CHEN W. & HUANG R.-H. 2006. Climate impacts of anthropogenic land use changes on the Tibetan Plateau. *Global and Planetary Change* **54**, 33–56.

DOMRÖS M. & PENG G. 1988. *The Climate of China*. Springer, Berlin.

DU M.-Y., KAWASHIMA S., YONEMURA S., ZHANG X.-Z. & CHEN S.-B. 2004. Mutual influence between human activities and climate change in the Tibetan Plateau during recent years. *Global and Planetary Change* **41**, 241–9.

FAN G.-Z., ZHANG T.-J., JI J.-J., LI K.-R. & LIU J.-Y. 2007. Numerical simulation of the carbon cycle over the Tibetan Plateau, China. *Arctic, Antarctic, and Alpine Research* **39**, 723–31.

FANG X.-M., LÜ L.-Q., MASON J. A. *et al.* 2003. Pedogenic response to millennial summer monsoon enhancements on the Tibetan Plateau. *Quaternary International* **106–107**, 79–88.

FENG Z.-D., AN C.-B. & WANG H.-B. 2006. Holocene climatic and environmental changes in the arid and semi-arid areas of China: A review. *The Holocene* **16**, 119–30.

FOOD AND AGRICULTURE ORGANIZATION OF THE UNITED NATIONS. 2006. *Guidelines for Soil Description*, 4th edn, UN Food and Agriculture Organization, Rome.

HERZSCHUH U. 2006. Palaeo-moisture evolution in monsoonal Central Asia during the last 50 000 years. *Quaternary Science Reviews* **25**, 163–78.

HERZSCHUH U., WINTER K., WÜNNEMANN B. & LI S. 2006. A general cooling trend on the central Tibetan Plateau throughout the Holocene recorded by the Lake Zigetang pollen spectra. *Quaternary International* **154/155**, 113–21.

INSTITUTE OF ARCHAEOLOGY OF THE CHINESE ACADEMY OF SOCIAL SCIENCES AND THE BUREAU OF CULTURAL RELICS OF THE TIBET AUTONOMOUS REGION. 1999. *Qugong in Lhasa: Excavations of an Ancient Site and Tombs*. China Publishing House, Beijing (in Chinese).

INSTITUTE OF GEOGRAPHY, CHINESE ACADEMY OF SCIENCES (ed.). 1990. *Atlas of Tibet Plateau*. Institute of Geography, Chinese Academy of Sciences, Beijing (in Chinese).

IUSS-ISRIC-FAO. 2006. *World Reference Base for Soil Resources. A Framework for International Classification, Correlation and Communication. World Soil Resources Reports* 130, 128. UN Food and Agriculture Organization, Rome.

KAISER K. 2007. *Soils and Terrestrial Sediments as Indicators of Holocene Environmental Changes on the Tibetan Plateau*. Habilitation thesis, Faculty of Geography, University of Marburg.

KAISER K., MIEHE G., SCHOCH W. H., ZANDER A. & SCHLÜTZ F. 2006. Relief, soil and lost forests: Late Holocene environmental changes in southern Tibet under human impact. *Zeitschrift für Geomorphologie Supplement* **142**, 149–73.

KAISER K., SCHOCH W. H. & MIEHE G. 2007. Holocene paleosols and colluvial sediments in Northeast Tibet (Qinghai Province, China): Properties, dating and paleoenvironmental implications. *Catena* **69**, 91–102.

KLEBER A. 2006. 'Kolluvium' does not equal 'colluvium'. *Zeitschrift für Geomorphologie* **50**, 541–2.

KLINGE M. & LEHMKUHL F. 2003. Paleosols and aeolian mantles in southern and eastern Tibet—Results and implications for Late Quaternary climatic change. *Berliner Paläobiologische Abhandlungen* **2**, 62–4.

KLOOTWIJK C. T., GEE J. S., PEIRCE J. W., SMITH G. M. & MCFADDEN P. L. 1992. An early India-Asia contact; paleomagnetic constraints from Ninetyeast Ridge, ODP Leg 121. *Geology* **20**, 395–8.

KRETSCHMER W., ANTON G., BENZ M. *et al.* 1998. The Erlangen AMS facility and its applications in ^{14}C sediment and bone dating. *Radiocarbon* **40**, 231–8.

KUHLE M. 2005. Glacial geomorphology and ice ages in Tibet and the surrounding mountains. *Island Arc* **14**, 346–67.

KÜSTER Y., HETZEL R., KRBETSCHEK M. & TAO M.-X. 2006. Holocene loess sedimentation along the Qilian Shan (China): Significance for understanding the processes and timing of loess deposition. *Quaternary Science Reviews* **25**, 114–25.

LAI Z.-P. & WINTLE A. G. 2006. Locating the boundary between the Pleistocene and the Holocene in Chinese loess using luminescence. *Holocene* **16**, 893–9.

LAI Z.-P., WINTLE A. G. & THOMAS D. S. G. 2007. Rates of dust deposition between 50 ka and 20 ka revealed by OSL dating at Yuanbao on the Chinese Loess Plateau. *Palaeogeography, Palaeoclimatology, Palaeoecology* **248**, 431–9.

LEHMKUHL F. & HASELEIN F. 2000. Quaternary palaeoenvironmental change on the Tibetan Plateau and adjacent areas (Western China and Western Mongolia). *Quaternary International* **65–66**, 121–45.

LEHMKUHL F., KLINGE M. & LANG A. 2002. Late Quaternary glacier advances, lake level fluctuations and aeolian sedimentation in Southern Tibet. *Zeitschrift für Geomorphologie Supplement* **126**, 183–218.

LEHMKUHL F. & OWEN L. A. 2005. Late Quaternary glaciation of Tibet and the bordering mountains: A review. *Boreas* **34**, 87–100.

LEOPOLD M. & VÖLKEL J. 2007. Colluvium: Definition, differentiation, and possible suitability for reconstructing Holocene climate data. *Quaternary International* **162–163**, 133–40.

LI X.-O., YI C.-L., CHEN F.-H., YAO T.-D. & LI X. 2006. Formation of proglacial dunes in front of the Puruogangri Icefield in the central Qinghai–Tibet Plateau: Implications for reconstructing paleoenvironmental changes since the Lateglacial. *Quaternary International* **154–155**, 122–7.

LIU J., SHEN X.-H. & XU Y.-R. 2007. West-northwest active fault and left-lateral displacement in Lhasa area, Tibet. *In* Aitchison J. C. (ed.). *Abstract volume of the 22nd Himalaya-Karakoram-Tibet Workshop*, Hong Kong, May 23–25, 2007, p. 62.

LIU Z.-M. & ZHAO W.-Z. 2001. Shifting sand control in Central Tibet. *Ambio* **30**, 376–80.

MIEHE G., MIEHE S., KOCH K. & WILL M. 2003. Sacred Forests in Tibet. Using geographical information systems for forest rehabilitation. *Mountain Research and Development* **23**, 324–8.

MIEHE G., MIEHE S., SCHLÜTZ F., KAISER K. & DUO L. P. 2006. Palaeoecological and experimental evidence of former forests and woodlands in the treeless desert pastures of Southern Tibet (Lhasa, A.R. Xizang, China). *Palaeogeography, Palaeoclimatology, Palaeoecology* **242**, 54–67.

MIEHE G., MIEHE S., WILL M. *et al.* 2008. An inventory of forest relics in the pastures of Southern Tibet (Xizang A.R., China). *Plant Ecology* **194**, 157–77.

MIEHE G., WINIGER M., BÖHNER J. & ZHANG Y.-L. 2001. The climatic diagram map of High Asia. Purpose and concepts. *Erdkunde* **55**, 94–7.

MONTGOMERY D. R., HALLET B., LIU Y.-P. *et al.* 2004. Evidence for Holocene megafloods down the Tsangpo River gorge, southeastern Tibet. *Quaternary Research* **62**, 201–7.

MORRILL C., OVERPECK J. T., COLE J. E., LIU K.-B., SHEN C.-M. & TANG L.-Y. 2006. Holocene variations in the Asian monsoon inferred from the geochemistry of lake sediments in central Tibet. *Quaternary Research* **65**, 232–43.

MURRAY A. S. & WINTLE A. G. 2000. Luminescence dating of quartz using an improved single-aliquot regenerative-dose protocol. *Radiation Measurements* **32**, 57–73.

OVERPECK J., LIU K.-B., MORRILL C. *et al.* 2005. Holocene environmental change in the Himalayan-Tibetan Plateau region: Lake sediments and the future. *In* Huber U. M., Bugmann H. K. M. & Reasoner M. A. (eds). *Global change and Mountain Regions: An Overview of Current Knowledge*.

Advances in Global Change Research 23, pp. 83–92. Springer, Boston, Massachusetts.

OWEN L. A., FINKEL R. C., MA H.-Z. & BARNARD P. L. 2006. Late Quaternary landscape evolution in the Kunlun Mountains and Qaidam Basin, Northern Tibet: A framework for examining the links between glaciation, lake level changes and alluvial fan formation. *Quaternary International* **154–155**, 73–86.

PESSENDA L. C. R., GOUVEIA S. E. M. & ARAVENA R. 2001. Radiocarbon dating of total soil organic matter and humin fraction and its comparison with ^{14}C ages of fossil charcoal. *Radiocarbon* **43**, 595–601.

PORTER S. C. & ZHOU W.-J. 2006. Synchronism of Holocene East Asian monsoon variations and North Atlantic drift-ice tracers. *Quaternary Research* **65**, 443–9.

PYE K. 1995. The nature, origin and accumulation of loess. *Quaternary Science Reviews* **14**, 653–67.

ROWLEY D. B. 1996. Age of initiation of collision between India and Asia: A review of stratigraphic data. *Earth and Planetary Science Letters* **145**, 1–13.

SCHARF A., UHL T., LUPPOLD W. *et al.* 2007. Status report on the Erlangen AMS facility. *Nuclear Instruments and Methods in Physics Research B* **259**, 50–6.

SCHOCH W. H. 1986. Wood and charcoal analysis. *In* Berglund B. E. (ed.). *Handbook of Holocene Palaeoecology and Palaeohydrology*, pp. 619–26. Wiley, Chichester.

SCHWEINGRUBER F. H. 1990. *Anatomy of European Woods*. Haupt, Bern.

SHEN X.-H., CAO Z.-Q., CHEN Z.-W., LIU J. & XU Y.-R. 2007. *Active Fault Detection and Seismic Hazard Evaluation in Lhasa*. Unpublished project report. China Earthquake Administration, Beijing (in Chinese).

SHI Y.-F., YU G., LIU X.-D., LI B.-Y. & YAO T.-D. 2001. Reconstruction of the 30–40 ka BP enhanced Indian monsoon climate based on geological records from the Tibetan Plateau. *Palaeogeography, Palaeoclimatology, Palaeoecology* **169**, 69–83.

SUN J.-M., LI S.-H., MUHS D. R. & LI B. 2007. Loess sedimentation in Tibet: Provenance, processes, and link with Quaternary glaciations. *Quaternary Science Reviews* **26**, 2265–80.

SWITZER A. D., JONES B. G. & AITCHISON J. C. 2007. Sedimentology and morphology of a barchan dune from Xigaze, Tibet. *In* Aitchison J. C. (ed.). *Abstract volume of the 22nd Himalaya-Karakoram-Tibet Workshop*, Hong Kong, May 23–25, 2007, p. 92.

TANG L.-Y., SHEN C.-M., LIU K.-B. & OVERPECK J. T. 2000. Changes in South Asian monsoon: New high-resolution paleoclimatic records from Tibet, China. *Chinese Science Bulletin* **45**, 87–90.

THOMPSON L. G., YAO T., MOSLEY-THOMPSON E., DAVIS M. E., HENDERSON K. A. & LIN P.-N. 2000. A high-resolution millennial record of the South Asian monsoon from Himalayan ice cores. *Science* **289**, 1916–19.

WENINGER B., JÖRIS O. & DANZEGLOCKE U. 2007. *CalPal-2007. Cologne Radiocarbon Calibration & Palaeoclimate Research Package*. [Cited 5 December 2007] Available from: http://www.calpal.de

WU Y.-H., LÜCKE A., JIN Z.-D. *et al.* 2006. Holocene climate development on the central Tibetan Plateau: A sedimentary record from Cuoe Lake. *Palaeogeography, Palaeoclimatology, Palaeoecology* **234**, 328–40.

ZHANG D.-D. 1998. Geomorphological problems of the middle reaches of the Tsangpo River, Tibet. *Earth Surface Processes and Landforms* **23**, 889–903.

ZHANG D.-D. 2001. Tectonically controlled fluvial landforms on the Yaluzangbu River and their implications for the evolution of the river. *Mountain Research and Development* **21**, 61–8.